THERMAL MASS FLOW MEASUREMENT

by

Gabriel J. Duffy, B.Eng.

A thesis submitted to

Dublin City University

for the degree of

Master of Engineering

SCHOOL OF ELECTRONIC ENGINEERING

DUBLIN CITY UNIVERSITY

August 2000

DECLARATION

I hereby certify that this material, which I now submit for assessment on the programme of study leading to the award of *Master of Engineering* (by research) is entirely my own work and has not been taken from the work of others save and to the extent that such work has been cited and acknowledged within the text of my work

Signed 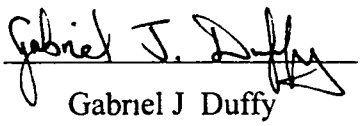 ID No 94971200

Gabriel J Duffy

Date 22nd May 2000

ABSTRACT

THERMAL MASS FLOW MEASUREMENT

This thesis presents a comprehensive static model for a capillary type thermal mass-flow sensor for gases Using such a sensor, a meter is constructed which measures gas mass flow by means of a bypass arrangement which ensures a constant flow ratio between the sensor and the meters' main flow element

The model equations are derived using steady state heat transfer theory for both a simplified one-dimensional and a multi-region two-dimensional case Consideration of a two-dimensional model allows for the analysis of additional model parameters such as gas conductivity and heat loss However for such a model, the use of analytical methods to obtain a system solution is precluded due to the complexity of the system, and hence a numerical discretisation method, namely the finite difference scheme, is employed to compute the temperature field for the multiregional system Heating coils are used to heat the sensor tube and are included in a bridge arrangement The mass flow rate, as indicated by the instrument, is calculated as a function of the bridge voltage as detected by the coils, which also function as thermal sensors

A reduced model is developed by omitting negligible model terms Such a model may be then used as a design tool for the simulation and optimisation of the performance of the flow meter

Actual test rig results are used to validate the model and both sets of results correlate well for low mass flow rates However, there remains a noticeable difference between the two for the non-linear sections of the output curve and the reason for this remains to be ascertained Nevertheless, the model has proved beneficial in showing the effect of parameter changes and the sensor's susceptibility to ambient temperature changes

Recommendations for future development and improvement are listed

ACKNOWLEDGEMENTS

First of all I would like to express my sincere thanks and gratitude to my supervisor Mr Jim Dowling for his help and support throughout the duration of this research project

Merci à Célia de m'avoir bien motivé et en plus de m'avoir poussé de terminer la thèse une fois pour toutes, même si l'on s'engueulait beaucoup trop à cause de cela

Thanks are also due to Dr Vernon Kirby of the School of Mathematical Sciences for his advice with the finer points of mathematics, and to the School of Electronic Engineering in general for advice, equipment, and humour

I would like to thank Unit Instruments Irl for the use of their equipment and for making measurement data available to me

Thanks also to my large circle of family and friends at home, in Dublin and abroad, for making the period in DCU so enjoyable and seem so short

Last but not least, I would like to thank PEI Technologies, a division of Forbairt, for their financial assistance and support, and in particular the PEI-DCU staff
Kevin Davis,
Liam Sweeney,
George Keenan

TABLE OF CONTENTS

CHAPTER 1

INTRODUCTION

1.1 Introduction

The purpose of any measuring system is to provide an observer with a numerical value corresponding to the variable being measured [1] All such variables are quantified in terms of seven fundamental and two supplementary physical units which include length, mass, time, and amount of substance

Mass and volume are among the macroscopic properties that all matter possesses Volume measurement presents few difficulties as one can pour the measurand into a container of known dimensions to obtain an answer at constant pressure and temperature In flow situations, to quantify mass, one needs to apply a force to the object whose mass is desired, measure the resulting acceleration, and utilise Newton's second law This complication has led to research for methods which infer rather than directly measure mass, particularly for fluids [2]

The study of fluids can be traced back to the second century BC to some of the earliest discoveries in physics One thinks of pioneers such as Archimedes, Pascal, Newton, and the multi-disciplinarian Leonardo da Vinci for important discoveries in the field of fluid dynamics [3] Flow metering involves the measurement of the quantity or rate of flow of a moving fluid in a pipe or open channel [4] Specific interest lay in this area for the ancient Romans in their distribution of water through pipes and aqueducts [5]

Today flow metering, or flow rate measurement, is important for most industrial processes Gases, due to their thermal and compressible nature, need distinct methods to measure their flow rates Many process controls involve the metering of gases at a definite molar or mass flow rate to maintain efficient reactions This is especially true with regard to the brewing and semiconductor industries, for example, fermentation

and device fabrication on wafers respectively [6] Volumetric measurement is not suitable for gases in these applications as the density of the gas will change with either changing temperature or pressure Mass flow rate (MFR) measurement of a gas can be determined by simultaneous measurement of the volume flow rate and the gas density Direct mass flow measurement is preferable because it offers a measurement which is unaffected by density, pressure, temperature, conductivity, and viscosity As a result it is inherently superior to volumetric measurement The most direct way to establish the MFR of a gas is to use a primary (or "direct") method and capture and record the mass that flows in a fixed time interval Direct results may be achieved by several different methods [7]

Thermal mass flow meters (MFMs) are gaining increasing importance as they are very sensitive for measuring gas mass flow rates, and have experienced most use for low flow (since excessive heat is added at high flow rates, as explained later in section 2 3 1) The extra heat needed in high flow rate MFMs is to produce a measurable temperature differential while a lot of heat is being lost due to convection Thermal MFMs can be either immersible or capillary type and the latter is described below

The heart of every capillary type MFM and associated controller is the sensor This is made up of a thin capillary tube of high aspect ratio around which resistive heating coils are wound The sensor measures only a certain fraction of the flow for convenience and economic reasons (See Figure 1 1), while the main flow travels through a bypass [8] Flow is initiated through the sensor because of a pressure difference across the bypass One can think of the bypass arrangement as being analogous to a current shunt

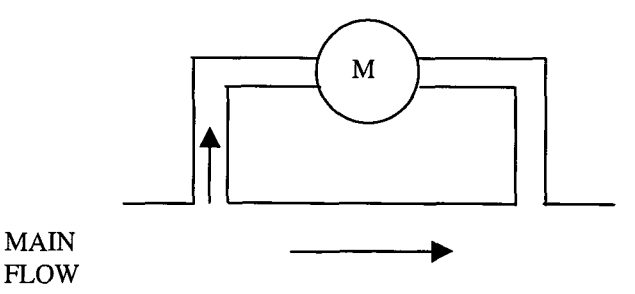

Figure 1.1 Bypass arrangement of MFM

1.2 Project specification and thesis details

Meters based on these capillary type sensors suffer from a need for costly individual calibration without appropriate attention being paid to the reason of this requirement This adds unwanted time and expense to the cost of the meter For optimal sensor (and meter) design a model is required that is sufficiently accurate to simulate the sensor Expertise can be gained faster and cheaper, without the need for costly trial-and-error experimental investigations Modelling may be considered a more time and economically efficient alternative approach

It was therefore decided to pursue the following tasks to ascertain the effectiveness and validity of such a model

- Preliminary research on the current state of mass flow meter technology
- Functional analysis of thermal type MFMs and in particular the capillary types and their sensors
- Model development of a capillary type MFM in detail which comprises models for both the sensor and the bypass arrangement in one-dimension (axial) only
- Validation of the model against experimental data
- Iterative attempts at model improvements, including two dimensional models if deemed necessary
- Drawing conclusions on completed work and making future recommendations

This thesis documents the static mathematical modelling of the aforementioned sensor Both one-dimensional and two-dimensional models were developed and actual recorded data is used to validate the models and simplifying assumptions The one-dimensional models proved to be enlightening with regard to the effect of parameter sensitivity whereas the two-dimensional models proved to be inconclusive despite the added complexity and there was no ascertainable difference between these and the former It is important to note that the measurements used throughout the thesis such as inches and sccms (standard cubic centimetres per minute) are the industry standard for gas flow sensor technology so no effort has been to change these to the international SI units

1.3 Outline of thesis

This thesis is divided into seven chapters as follows

Chapter 1 gives a brief introduction to the field of mass flow measurement, its history and its role in industry today

Chapter 2 presents descriptions of different methods of mass flow measurement with emphasis on thermal types, and in particular the capillary type bypass meter

Chapter 3 describes the initial static one-dimensional (1D) modelling of the sensor and discusses what may be learned from these model solutions Also included is a derivation of the bridge output voltage as a function of differential temperature along with a bypass model to allow complete simulation of the meter

A two-dimensional (2D) formulation of the problem is developed in chapter 4 and the equations are discretised and solved The merits of this model over the 1D model previously presented are shown Current mathematical software capable of solving systems of partial differential equations is listed A description of the code used and problems encountered is contained

Chapter 5 outlines the experimental determination of the sensor's characteristic curves for various gases A description of the test rig setup and its associated C code for the Loughborough Sound Images (LSI) PC system board and Texas Instruments TMS320C30 digital signal processor is included

In chapter 6 the models are validated with the experimental data obtained The limitations of the models are considered and the results analysed

Conclusions and recommendations for future work are given in chapter 7

CHAPTER 2

PRINCIPLES OF MASS FLOW METERS

2.1 Introduction

The mass flow marketplace today is expanding with no signs of market saturation [9] Mass flow rate measurement is widely employed in industry as mass and energy balances are important for many industrial processes The two main types of meter used are the thermal and Coriolis meters [10]

Thermal sensing types came on the scene in the late 1960s, the main driving force for this meter type being the semiconductor industry - low flows, difficult fluids and requirements for ultra precision and ultra purity This is where its relative strength over the former methods lie However these types did not give a direct measurement

The first commercial Coriolis meters were produced in the late 1970's Prior to this date, if mass flow rate was the desired measurand, one had to derive, rather than directly measure it Coriolis meters are used in the measurement of high pressure gases as the high pressures boost the viscosity and density of the gas to within the limits of the Coriolis sensing tubes [6]

2.2 Overview of mass flow meter types

Mass flow measurement techniques can be broadly divided under three main headings Direct, Indirect, and Thermal

2.2.1 Direct methods

A true or direct measurement of mass flow rate for a fluid provides a measure of the mass independent of the properties and the state of the fluid The meter's response is

therefore a function of mass flow rate only A number of methods of achieving this exist

1) Coriolis method

The principal mass flow measurement technology is known to be the Coriolis mass flowmeter which was pioneered by a company from Colorado in the USA named Micro Motion, Inc in 1971 It offers very good reliability and precision and covers a wide range of substances (fluid and solid) and conditions At present it is most suitable only for high pressure gases [9,10,11]

A Coriolis force results when a mass in a rotating body moves relative to the body in a direction that is either towards or away from the centre of rotation The mass will experience two components of acceleration, a centripetal acceleration acting away from the centre of rotation, and a Coriolis acceleration which is perpendicular to the former A common illustration is the example of a person walking radially outward on a merry-go-round having to lean against the Coriolis force to maintain his/her balance The Coriolis acceleration C_a may be shown to be equal to $2\omega v$ where ω is the angular velocity of the body, and v is the radial velocity of the mass [9]

One form of meter takes the form of Figure 2 1 below [4] A torque measurement of the motor is made while maintaining a constant motor angular velocity (ω) The rotor has radial vanes attached so that the fluid is forced to experience a Coriolis force This is detected as a load torque on the motor since the force acts in the plane of rotation of the motor The mass flow rate is directly proportional to the load torque

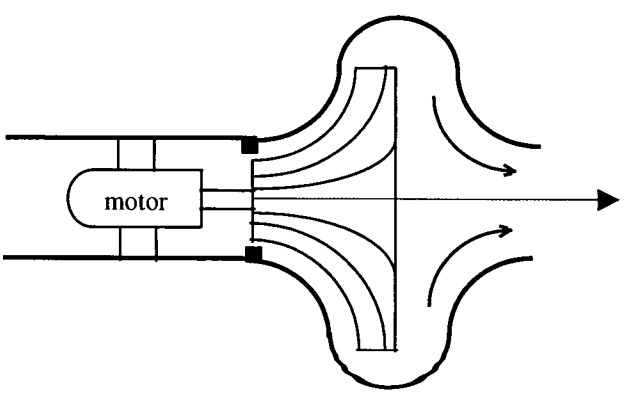

Figure 2.1 Coriolis MFM

A more practical and modern Coriolis meter dispenses with the idea of using a motor to create a rotating body Instead the tube is vibrated close to its natural frequency An oscillating torque is produced from which the mass flow rate may be derived The main difference between these new commercially available meters are the size and shape of the vibrating element [7]

2) Gyroscopic method

This type also utilises the effect of Coriolis acceleration [4,7] The difference between this and the Coriolis meter is the plane of rotation relative to the plane of the resulting torque For the Coriolis meter we have seen in the previous section that the torque acts in the plane of rotation In the case of the gyroscopic meter the fluid passes through a tube which is ring-shaped about the shown Z-axis in Figure 2 2 The inlet and outlet of the meter are on the X-axis about which the meter is rotated at angular velocity ω Gyroscopic precession occurs with the flowing fluid trying to rotate along the Y-axis An output torque can thus be measured along the Y-axis from the ensuing twist perpendicular to the plane of rotation The gyroscopic meter is usually vibrated about the X-axis as it is more convenient than having continuous rotation It also eliminates the need for rotating seals

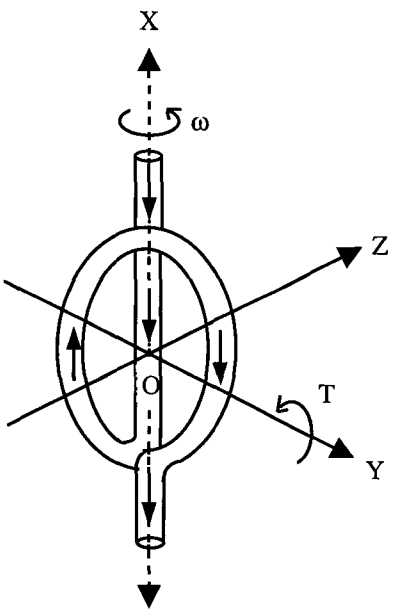

Figure 2.2 Gyroscopic MFM

3) Magnus effect method

This method is dependent on inducing a circulation of the fluid as in Figure 2 3 A cylindrical rotor spins at a constant angular velocity ω within the outer casing As the flow of fluid, travelling initially with a velocity V, passes by the rotor a pressure differential ΔP builds between P_1 and P_2 [7] This is a result of a local increase and decrease in velocity below and above the rotor respectively The mass flow rate may be measured as a linear function of ΔP

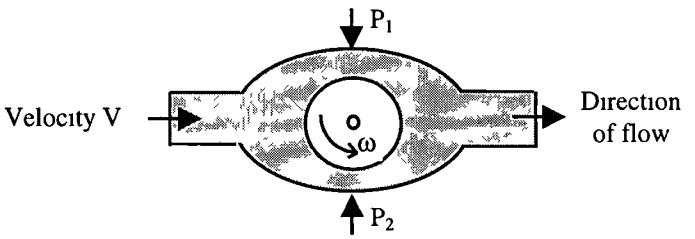

Figure 2.3 Magnus effect meter

4) Momentum change methods

A general layout for an angular momentum change flowmeter is shown in Figure 2 4 The fluid follows the path indicated by the dotted line and flows through the impeller followed by the turbine It obtains an angular momentum going through the vaned impeller which is travelling at angular speed ω As the fluid flows through the turbine, it attempts to impose its acquired swirling motion upon it To prevent the turbine also rotating at angular speed ω, it is decoupled from the impeller and also restrained at its other end by a spring [12,13] Since the turbine is restrained, all the energy imparted on the fluid by the motor is dissipated in the turbine and the flow straightened A reaction torque measurement (T) is obtained from the restraining force necessary by the spring The mass flow rate can be expressed in an equation of the form $m=K\ (T/\omega)$ where K is a constant It is assumed that the fluid contained no angular momentum prior to entry into the meter as the velocity term of the equation denotes its change From the equation we see that there are two possible modes of operation with this meter ω may be held constant and T measured, or vice versa

In theory a turbine is not necessary and may be eliminated, as one may measure the load torque on the rotor instead In this scenario a motor may be built in to the main

flow path with its stator residing outside of the flow tube. The major disadvantage to this method in general is the number of rotating parts which all require maintenance. Linear momentum mass flowmeters are also coming onto the market. They involve the measurement of a restraining torque in the axial direction [14].

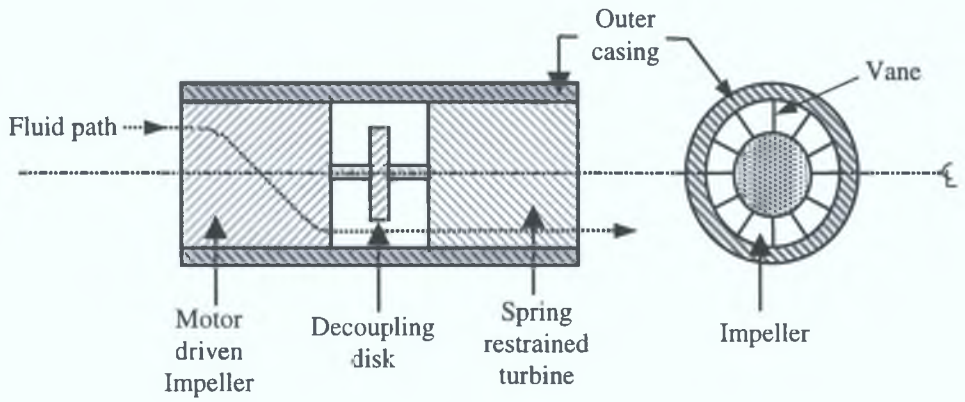

Figure 2.4 Momentum change meter

5) Flow injection and subtraction (Pressure differential) method

Fluid flow is split between into two equal flow paths in a form analogous to that of a Wheatstone bridge circuit as in Figure 2.5. The flow is increased in one path at the expense of the other by the use of the independently driven positive-displacement pump. From the pressure differential created across the pump (ΔP), the mass flow $\dot{m}$ can be determined.

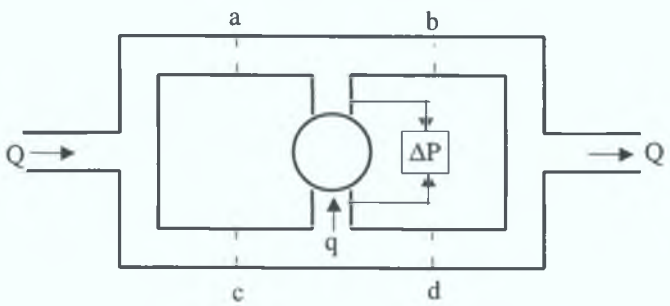

Figure 2.5 Pressure differential meter

The four orifices a, b, c, and d are an identical size, the pressure drop across each being proportional to ρQ^2, where Q is the volumetric flow rate and ρ is the density of the fluid. This eases the solution of equations and an expression for mass flow rate can be derived that is directly proportional to ΔP[13,15]:

The above method assumes that q is less than Q The pressure measurement is taken across the inlet and outlet of the arrangement if q happens to be larger than Q, this method is used only with liquids

2.2.2 Indirect methods

Another approach available is to use an indirect or inferential method This involves the simultaneous measurement of quantities from which the mass flow rate is derived Some of these methods are presented below

1) Flowmeter with densitometer method

In this method the mass flowrate is computed by finding the product of density and volumetric flow rate [15,16,17] Some of the main flow is bypassed to get a direct density measurement as in Figure 2 8 Care must be taken to ensure that the same fluid conditions apply for both meters and that the fluid output from the densitometer doesn't interfere with satisfactory volumetric flowmeter operation An alternative arrangement of the above utilises secondary measurement of the inlet temperature and pressure to calculate the density by way of the ideal compressible gas law

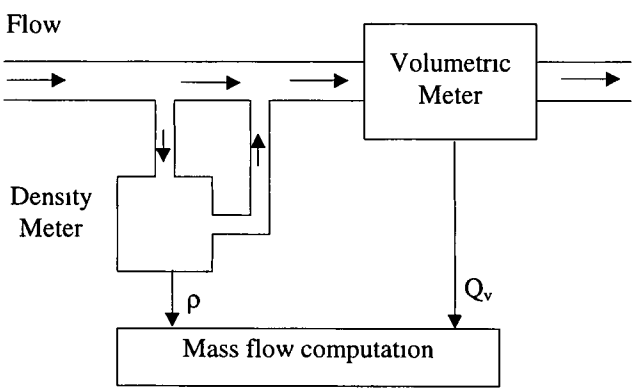

Figure 2.8 MFM with densitometer

2) Critical orifices method

Critical orifices are also known as sonic nozzles [18] The upstream pressure P_1 is kept at approximately twice the throat pressure P_2, which ensures the gas then reaches its sonic velocity regardless of the inlet pressure The mass flow rate can be found to

be directly proportional to the upstream pressure P_1 This method is usually used for transfer standards

2.3 Thermal types:

2.3.1 Outline of thermal types

Thermal MFMs can be used to measure large ranges of flow, but are usually confined to low flow due to the excessive expended energy at high flow rates [19]

They are not considered to be true mass flow meters as they respond to secondary parameters such as viscosity, specific heat and thermal conductivity of the fluid Consequently many measurements are in essence combined to give the mass flow rate which illustrates its inferential nature However in cases where there is small temperature variance and possibly compensation by signal processing, the measurements veer from an inferential type towards the direct one claimed by MFM and mass flow controller (MFC) manufacturers such as Unit Instruments and Sierra Instruments in their advertising brochures [20,21]

In the thermal class of flowmeters, the flow rate can be measured by either monitoring the cooling action of a fluid on a heated element or by the transfer of heat energy between two points in the flow path

2.3.2 Insertion/Immersion type

Insertion/Immersion measurement systems (also known as hot wire or hot film techniques depending on the sensor type) have two sensors that are inserted into the flowing gas as in Figure 2 9 One of the sensors monitors the gas temperature, while the other is heated and monitors the mass flowrate Each sensor is a resistive temperature detector A temperature difference ΔT is computed along with the heat loss, H, by the heated sensor to the fluid Taking K to be a constant, the mass flowrate can be shown to be [12]

$$m = K\left(\frac{H}{\Delta T}\right)^{1.67} \qquad \text{Equation 2 1}$$

The drawback to this method is that it cannot be utilised in situations where hazardous gases are used as the heated element is inserted directly into the gas A meter that is capable of overcoming this fault is described in section 2 3 3 Insertion types are usually calibrated for one gas only due to the inherent danger mentioned previously The sensors also present a slight obstruction to flow that causes the heated sensor to record a slight positive error This depends very much on the shape of the sensor [22] The advantage of these meters lies in their fast response times and the fact that they may be used for high flow ranges

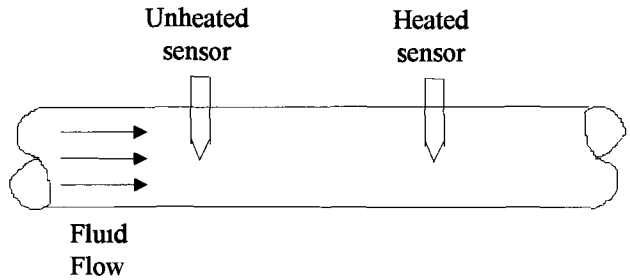

Figure 2.9 Insertion meter

2.3.3 Capillary Tube Thermal Mass Flow Meter

Figure 2 10 below shows a capillary tube mass flow controller that is composed of an MFM and some associated control circuitry This is a model readily available from a company named Unit Instruments

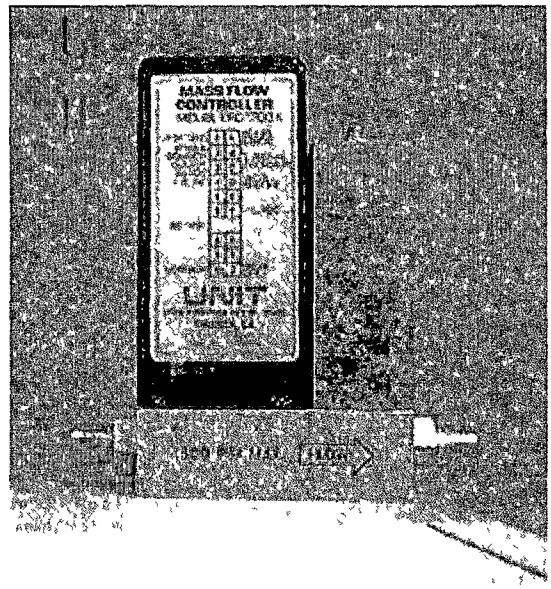

Figure 2.10 Unit Instruments MFC

Figure 2.11 shows a meter without the external cover from which we can clearly identify the main flow element with the 'flow arrow', the valve unit (above on the

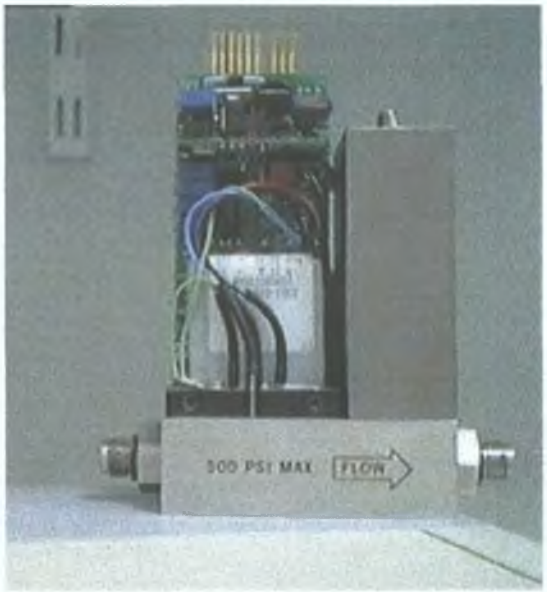

Figure 2.11 PCB circuitry

right hand side), the printed circuit board (PCB), and finally the capillary tube sensor itself which is located directly in front of the PCB. Finally, Figure 2.12 shows a close up of the sensor. One can see that this is a completely insulated and sealed unit with only the electrical connections protruding. The gas input and output are located below and fit into the base piece.

Figure 2.12 Close-up of sensor

Figure 2.13 shows the general layout of a typical capillary tube MFM. This works on the basic principle that every gas molecule has the ability to absorb heat energy. This ability, known as specific heat, is directly related to the mass and physical structure of the molecule [23].

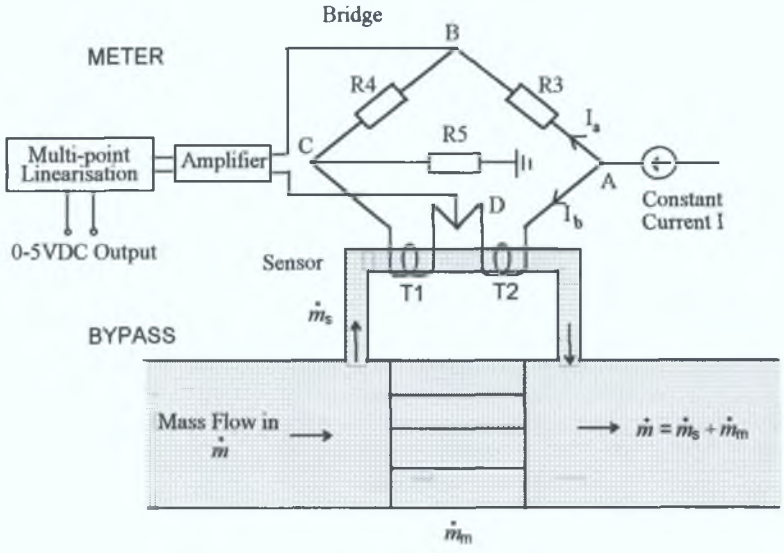

Figure 2.13 MFM block diagram

Flow is initiated through the sensor tube because of a pressure difference created by the bypass element. The flow through the sensor tube is always small, usually a small fraction of the total mass flow. The mass flow is divided proportionally between the sensor tube and the bypass, $\dot{m}_m = C\dot{m}_s$. This proportion must remain constant for the MFM to be accurate; for this the flow must remain laminar through the bypass and the sensor. For laminar flow the Reynolds number should be less than 2000 [24]. To ensure this, the length to diameter ratio of the sensor is typically in the range 50:1 to 100:1. Otherwise if turbulent flow exists, temperature measurements are inconsistent and the flow splitting ratio is not applicable. The reason this proportionality exists is because the relationship between flowrate and the pressure drop in the sensor follows a square law, which is approximately cancelled out by the square-root effect in the bypass itself [16]. This is discussed later in section 3.3.

An additive energy approach is used in that the coils around the sensor provide a constant heat source to it [25]. A constant amount of electrical power from a constant current supply to the bridge provides a constant heat source Q. A Wheatstone bridge is used where the two coils form one of the arms [26]. It is assumed that all the heat generated is supplied to the gas through the thin walls of the sensor, and that there is

no heat loss as the sensor and coils are surrounded by a layer of insulation The walls of the sensor are kept as thin as possible to ensure that as much of the heat as possible is transferred to the gas to produce a greater temperature differential and to minimise the time response of the meter thus improving its dynamic characteristics

The coils have a dual role in that they act as both gas heating and resistance-temperature detector elements They are, in effect, temperature compensated as any change in ambient temperature affects both coils to the same degree The temperature difference is transduced into an analogous form, a voltage

Since the coils are symmetrically located around the centre point of the sensor, at zero mass flow, the temperature distribution across the sensor is also symmetric This results in a zero differential temperature $\Delta T = T_2 - T_1$ being detected (where T_1 and T_2 are the average temperatures in each of the coils) An inverse relationship exists between the differential temperature and the mass flow rate as given by equation 2 2

$$\Delta T = Q/mC_p \qquad \text{Equation 2 2}$$

This is due to the first law of thermodynamics where energy cannot be created or destroyed the heat added, Q, is equal to the heat convected away at a mass flowrate m Thomas used this law for the design of his flowmeter in 1911 [21,27] It is dependent on heat supplied remaining constant (See Figure 2 14)

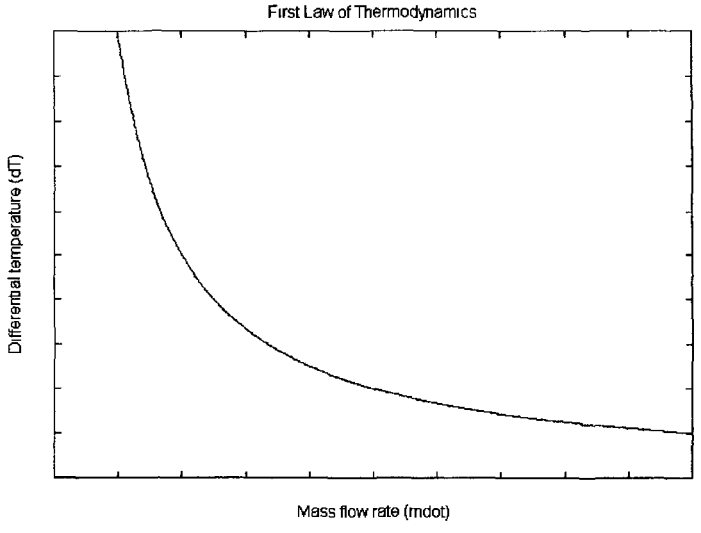

Figure 2.14 Relationship between differential temperature and mass flow rate

Figure 2.15 shows the general temperature distribution curves against fractional length of sensor obtained by use of models developed in chapter 3. From the diagram it can be seen that at high flow rates, there is a large difference in temperatures at these points. (Assuming that the average temperature of coils 1 and 2 are represented at points 0.25 and 0.75 respectively on the fractional length axis.)

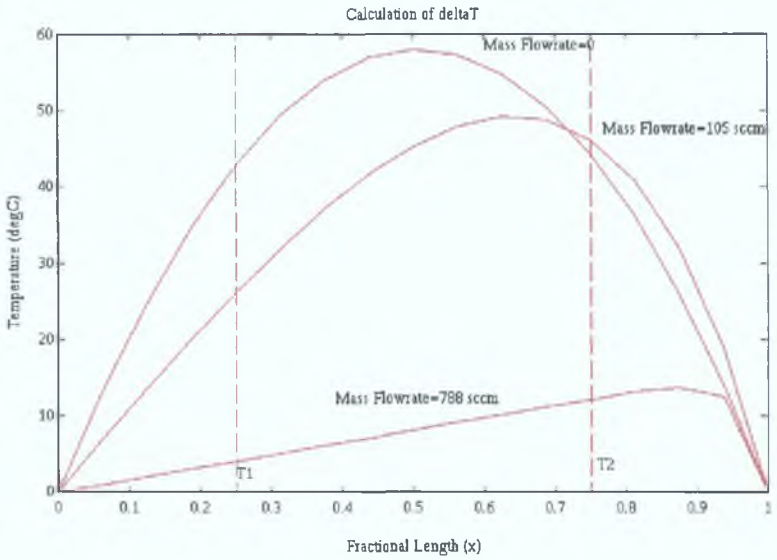

Figure 2.15 Temperature profile along sensor

Figure 2.16 shows a typical plot of ΔT against mass flowrate for the aforementioned model using nitrogen gas. Note that this curve is variable and dependant on many separate parameters relating to the many gases for which the meter is calibrated and to the sensor itself. Therefore it is necessary to simulate the model for each and every gas and also when the sensor is changed. However, the general shape of the curve is always the same with the only difference being in the scaling of the typical curve in both the horizontal and vertical directions. The sensitivity of the output curve to changes in the gas and sensor properties such as conductivity, specific heat capacity, viscosity, and tolerances is discussed later on in the thesis in section 3.4.7.

It can be seen that at low flow rates the mass flowrate can be approximated as being directly proportional to ΔT. This is the design range of a MFM. For increased accuracy, multi-point linearisation may be used in the design range. This strategy, as used by many commercial vendors, divides the range into sections for which in each the output has a different constant of proportionality with the mass flow rate. It is

important to note that the turning point of the curve is the maximum mass flow rate for which an unambiguous measurement can be calculated. To ensure accuracy the gas must be 'dry' and contain no vapour, as errors will occur due to latent heat effects [25]. Entrained liquid may be removed by prior heating of the gas.

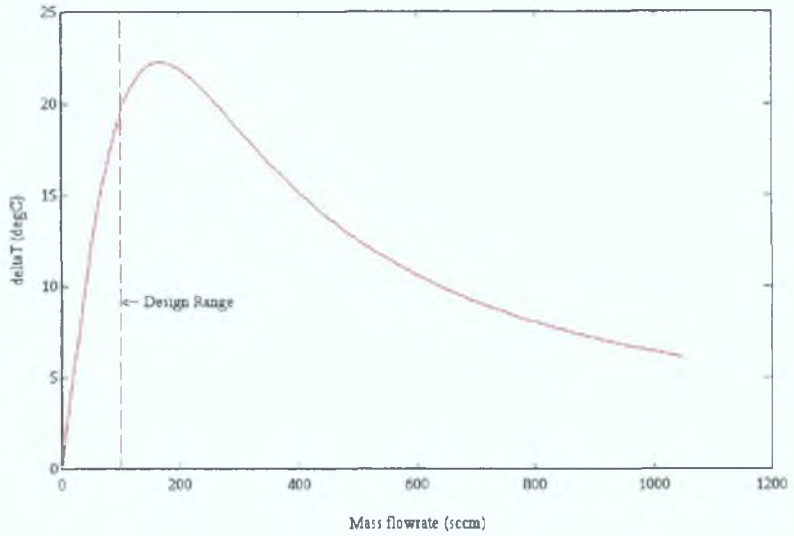

Figure 2.16 Typical meter output curve

An inherent advantage to this measurement approach is its non-intrusive nature and the fact that it can also be calibrated for different gases.

2.4 Summary

Many varieties of well established MFMs have been described in this chapter. All of the truly direct types are based solely on fluid-mechanical principles. Indirect methods simply involve a mathematical adjustment of an available volumetric mass flowrate. These may suffice for certain applications, but they are inherently less accurate than direct methods as they suffer from cumulative inaccuracies in the final calculation. No attempt is made to describe the countless volumetric flowmeters available.

Coriolis meters are generally not sufficiently sensitive enough for gases; their forte is in the measurement of liquid mass flows. Thermal techniques offer the best alternative for measuring gas mass flow rate but are unsuitable for two-phase flow. As such, they have made a major impact in the market of single phase flow meters.

CHAPTER 3

ONE-DIMENSIONAL (1-D) MODELLING

3.1 Introduction :

Our most utilised of physical laws today are nothing more than accurate models of physical systems Models can be qualitative or quantitative depending on the level of insight we require of the system Quantitative modelling can be subdivided into 'black box' and 'white box' types Black box modelling reduces the effort required, but little is known other than a predicted set of outputs for a given set of inputs If one requires detailed knowledge of the internal workings of the system, the system is described by differential equations and it is then termed a white box model [28]

This approach was adopted with regard to the meter as qualitative models based on user experience are not adequate for sensor design purposes The first step was to complete the preliminary work outlined earlier in the project specification in Chapter 1 to produce a simple one-dimensional sensor model and assess its validity The model was repeatedly increased in complexity with the 'correct' model being the simplest one that fits all the data Note that this model was being developed for an existing Unit Instruments E-type sensor [29] A derivation of the output voltage and a bypass model is shown to allow a complete meter simulation

3.2 Derivation of output voltage :

The output voltage provides a measurement proportional to the temperature difference between the two coils and also quasi-proportional to the mass flow rate through the sensor as will be later demonstrated With reference to Figure 3 1 it can be seen that $R_1 = R_0\left(1+\alpha\overline{T_1}\right)$ corresponds to coil 1 in the diagram where $\overline{T_1}$ is measured This

equation gives the resistance variation of R_1 with respect to temperature α is the thermal coefficient of resistance of the coil, R_0 is the coil resistance at ambient temperature, and $\overline{T}_1$ is the temperature rise or fall of the coil above or below ambient temperature This is an average temperature along the coil The equation for the second coil, $R_2 = R_0(1+\alpha\overline{T}_2)$, can be similarly explained From measurements at ambient temperature $R_0 = 55\Omega$ and $R_3 = R_4 = 20k\Omega$ for the E-type sensor used

The current through resistors R_3 and R_4 is I_a, given by

$$I_a = \frac{R_1 + R_2}{R_1 + R_2 + R_3 + R_4} I \qquad \text{Equation 3 1}$$

where I is provided by the constant current source I

The current through the sensor resistors (windings) R_1 and R_2 is I_b, given by

$$I_b = \frac{R_3 + R_4}{R_1 + R_2 + R_3 + R_4} I \qquad \text{Equation 3 2}$$

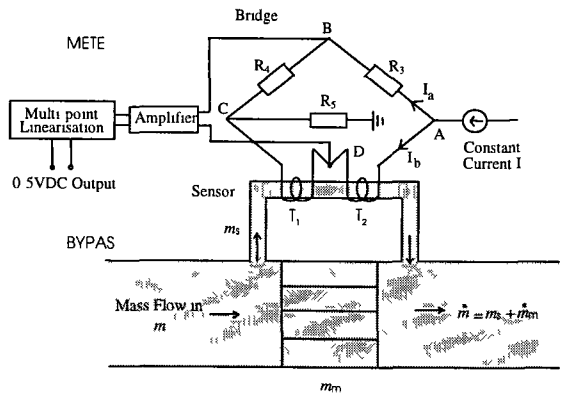

Figure 3.1 MFM block diagram showing bridge arrangement

The output voltage V_{OUT} required is V_{BD}

$$V_{OUT} = I_a R_4 - I_b R_1 \qquad \text{Equation 3 3}$$

$$= \frac{I[(R_1 + R_2)R_4 - (R_3 + R_4)R_1]}{R_1 + R_2 + R_3 + R_4} \qquad \text{Equation 3 4}$$

$$= \frac{I[R_0 R_3(2 + \alpha(\overline{T}_1 + \overline{T}_2)) - 2R_0 R_3(1 + \alpha\overline{T}_1)]}{R_0(2 + \alpha(\overline{T}_1 + \overline{T}_2)) + 2R_3} \qquad \text{Equation 3 5}$$

$$= \frac{I\alpha[\overline{T}_2 - \overline{T}_1]}{2 + \alpha(\overline{T}_1 + \overline{T}_2)/R_3 + 2/R_0} \qquad \text{Equation 3 6}$$

$$\Rightarrow V_{OUT} = \frac{I\alpha R_0 R_3 \left[\overline{T}_2 - \overline{T}_1\right]}{\left(2+\alpha\left(\overline{T}_1 + \overline{T}_2\right)\right)+2R_0R_3} \qquad \text{Equation 3 7}$$

Since

$$2R_3 >> R_0\left(2+\alpha\left(\overline{T}_1 + \overline{T}_2\right)\right) \qquad \text{Equation 3 8}$$

i e 40kΩ >> 170Ω (taking the sum of the temperatures to be a maximum of 200°C)

then

$$V_{OUT} \approx \frac{IR_0\alpha}{2}\left[\overline{T}_2 - \overline{T}_1\right] = 0\,007\left[\overline{T}_2 - \overline{T}_1\right] V \qquad \text{Equation 3 9}$$

(I was measured at 47mA and α is quoted as being 0 0054 °C ^{1}) [29]
Equation 3 9 gives the required relationship between the output of the bridge and the difference of the average temperature of the coils This voltage is then amplified to scale the maximum mass flow rate to a corresponding value of 5V

3.3 Bypass modelling :

A bypass model developed by Punch is summarised and shown to allow a complete meter simulation in conjunction with the thermal models completed later in this thesis [30] Its employment enabled the effect of the bypass on the meter's linearity to be seen and effectively demonstrates that the main source of non-linearity stems from the sensor

The bypass element is made up of a tube bundle, as shown in Figure 3 2, which is very effective at reducing swirl It also corrects an asymmetrical velocity profile but tends to flatten a correctly shaped profile Other types of bypass elements, such as étoile (cross section also shown in Figure 3 2), have negligible head losses and poor asymmetry correction [16,17]

The total meter flow m is a combination of the sensor flow m_s and the main flow though the bypass From the conservation of mass $m = m_s + m_m$ See Figure 3 1

CSA of tube bundle bypass CSA of étoile bypass

Figure 3.2 Different bypass types

As all the meter's mass flow passes through a parallel network of tubes, it is reasonable to assume that there exists an equipressure loss across each The Darcy-Weisbach head loss equation [5] applies in such situations and must be satisfied for each branch It may be given as

$h_{loss} = K_i \frac{u_i^2}{2g_c}$ where u_i and K_i are the average velocity and head loss coefficient in the i-th branch respectively g_c is the gravitational acceleration constant

3.3.1 Determination of head loss coefficient K_s in the sensor

The loss of pressure head (ΔP) across the sensor is given by $\Delta P = K_s \left(\frac{\rho u_s^2}{2} \right)$ where ρ is the density of the fluid, and u_s is the average velocity in the sensor K_s must take into account the loss of pressure by the horizontal tube, the two 90° bends, and the contraction and expansion at the inlet and outlet respectively As these tube elements are in series with one another, the overall head loss coefficient for the sensor is the additive total of all the above individual losses This can be seen quite clearly in equation 3 13

1) Head loss to friction by the horizontal tube

From the Darcy-Weisbach equation the head loss coefficient K for a straight horizontal tube may be given as $4fl/d$ where f is the dimensionless friction factor, l is the length, and d the diameter of the tube

As only laminar flow applies in both the sensor and the bypass, the friction factor is purely dependent on the Reynolds number of the flow within the tube and may be rewritten in terms of mass flow rate m_s as

$$f = \frac{16}{\mathrm{Re}} = 16\frac{\nu}{u_s d} = 4\frac{\nu\rho\pi d}{m_s} \qquad \text{Equation 3 10}$$

where ν is the kinematic viscosity of the fluid

The head loss coefficient across the tube becomes

$$K = 4\frac{\nu\rho\pi dl}{m_s d} = \frac{16\nu\rho\pi l}{m_s} \qquad \text{Equation 3 11}$$

Equation 3 11 also applies with regard to all the bypass tubes The important point to note is that it is a function of mass flow rate

2) Determination of head loss for the expansion, contraction and the bends

For an abrupt enlargement in a piping system from pipe diameter d_1 to pipe diameter d_2 the head loss coefficient can be shown to be

$$K = \left(1 - \left(\frac{d_1}{d_2}\right)^2\right)^2 \qquad \text{Equation 3 12}$$

A look up table is used to find the corresponding head loss coefficient for the abrupt contraction and a head loss coefficient of 0 5 is assumed for the smooth 90° bends [31] The total head loss coefficient for the sensor becomes

$$K_s = 0\,5 + 2\ \ 0\,5 + 1 + \frac{16\nu\rho\pi l}{m_s} \qquad \text{Equation 3 13}$$

(due to contraction, bends, expansion, and friction respectively)

It is assumed that the diameters of the sensor and the bypass tubes (0 4mm and 0 5mm) are much less than the main bore (12mm) of the meter block

The chief source of error in the analysis is the evaluation of the head loss coefficients because empirical correlations are only available for certain geometries [30]

3.3.2 Determination of head loss coefficient K_m for individual bypass tubes

With the assumption that all the bypass tubes are identical, the head loss coefficient for each individual tube can be derived in a similar manner to equation 3 13 and shown to be

$$K_m = 15 + \frac{16\nu\rho\pi l}{m_m} \qquad \text{Equation 3 14}$$

3.3.3 Relationship between sensor flow and meter flow

By equating the pressure losses in the sensor and the many bypass tubes the following relationship as developed by Punch is found [30]

$$m = m_s\left[1+\sum_{i=1}^{N}\left(\sqrt{\frac{K_s}{K_i}\frac{A_i}{A_s}}\right)\right] \qquad \text{Equation 3 15}$$

The variable i in equation 3 15 denotes an index for the number of bypass tubes, N A_s and A_i are the cross sectional areas of the sensor and a single bypass tube respectively K_s and K_m may be directly substituted into equation 3 15 from equations 3 13 and 3 14 to get the following relationship between the sensor flow and the total flow of the meter

$$m = m_s\left[1+N\left(\sqrt{\frac{2.5+\frac{16\rho\pi\nu l_s}{m_s}}{15+\frac{16N\rho\pi\nu l_{byp}}{m-m_s}}}\frac{A_{byp}}{A_s}\right)\right] \qquad \text{Equation 3 16}$$

Equation 3 16 is solved by iteration in Appendix A Figure 3 3 illustrates the negligible dependence of the flow ratio (bypass to sensor) to mass flow rate for a sample bypass consisting of five tubes with 0 020" (0 508mm) diameter This verifies the validity of the assumption that the sensor flow remains a constant fraction of the total meter flow regardless of the sensor flow Nevertheless this negligible non-linearity of the bypass arrangement in the meter could be easily compensated for by incorporating a linear approximation for the relationship between the flow ratio and the mass flow rate as in Fig 3 3

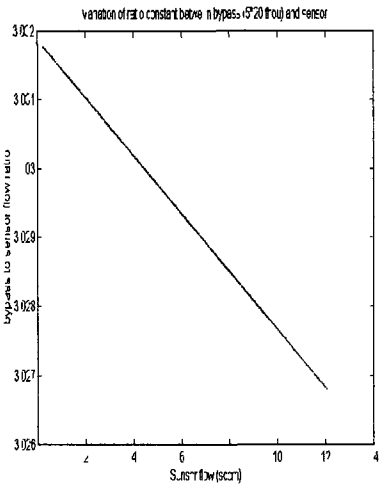

Figure 3.3 Relationship between the flow ratio and the mass flow rate

3.4 Sensor modelling :

Sensor models may be reduced to either static or dynamic types The conventional approach in modelling is to treat both separately The overall performance of the sensor may then be judged by a semiquantitative superposition of the static and dynamic characteristics All the models derived from here on are static (steady state)

3.4.1 Basic model

The modelling of the system was completed by considering a differential length *dX* along the length of the sensor that is assumed to be straight [32] See Figure 3 4

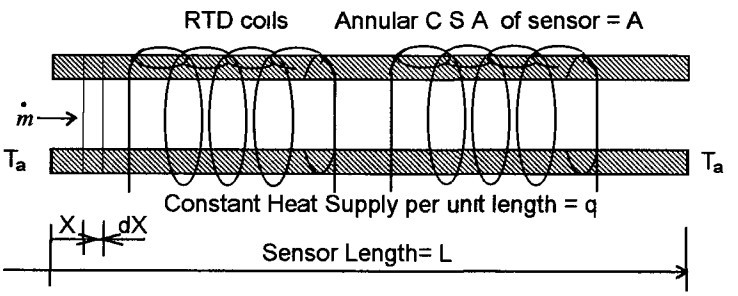

Figure 3.4 Sensor diagram

This gives a thermally symmetric parabolic temperature distribution as expected (See Figure 2.12) [33]. (Note: Parameter values are taken from an existing Unit Instruments E-type sensor [29]).

If the mass flow rate ($\dot{m}$) is now taken into account.

$$kAd\left(\frac{dT}{dX}\right) = -\dot{q}dX + \dot{m}C_p dT \qquad \text{Equation 3.20}$$

where C_p is the specific heat capacity of the gas.

This equation may be rewritten as

$$kA\frac{d^2T}{dX^2} - \dot{m}C_p\frac{dT}{dX} = -\dot{q} \qquad \text{Equation 3.21}$$

The solution to equation 3.21 with the boundary conditions being that $T = T_a$ @ x=0 and $T = T_a$ @ x=1 is given by equation 3.22.

$$T(x,\dot{m}) = T_a + \frac{\frac{\dot{q}}{\dot{m}C_p}L}{e^{(\dot{m}C_p/kA)L} - 1}\left(1 - e^{(\dot{m}C_p/kA)X}\right) + \frac{\dot{q}}{\dot{m}C_p}X \qquad \text{Equation 3.22}$$

Noting that $e^X = \sum_{n=0}^{\infty}\frac{X^n}{n!}$, one may use Taylor series expansions on equation 3.22 to arrive at equation 3.19 for zero mass flow calculated earlier. Figure 3.5 shows a plot of the bridge output voltage against mass flow rate for nitrogen gas. Figure 3.6 illustrates in mesh diagram format the changing temperature profile of the sensor for changing mass flow rate. Note that the temperature shown is $T - T_a$.

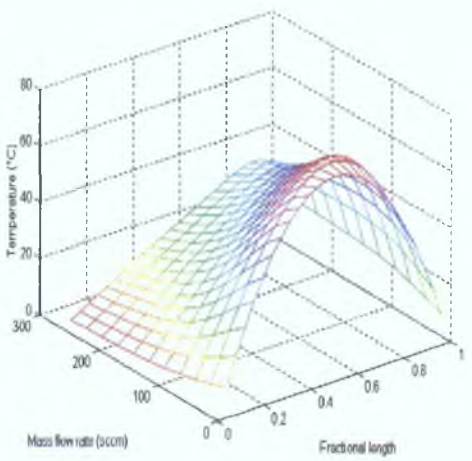

Figure 3.6 3D diagram of temperature distribution for changing mass flow rate

3.4.2 Explanation of shape of output curve

The explanation will be divided up into a number of sections for which certain key mass flow rates have been identified. These correspond to turning points on the output curve that is shown in Figure 3.7a. The average temperature of the coils is also shown. To aid the discussion it is also necessary to include other graphs that show the temperature derivatives with respect to mass flow rate of these temperature readings. These were computed by subtracting adjacent temperature data points. See Figure 3.7b. (NB Second derivatives are scaled by a factor of 20).

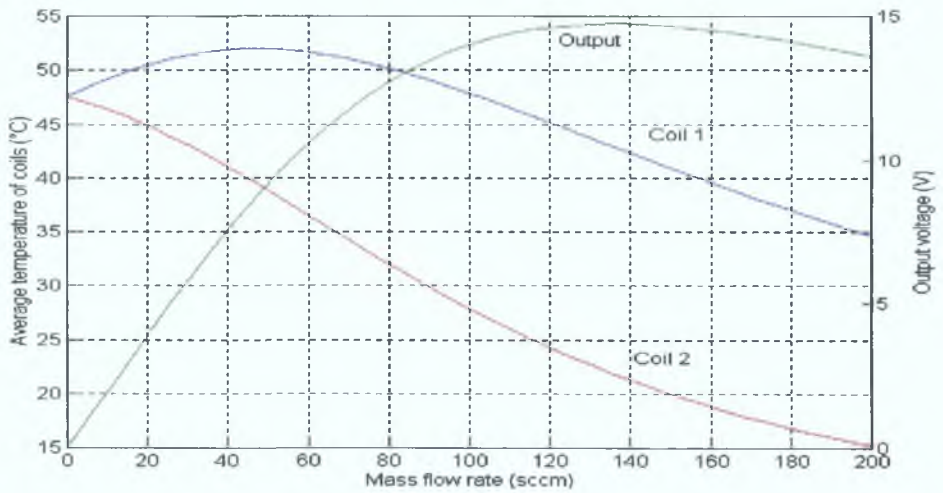

Figure 3.7a Coil temperatures for changing mass flow rates

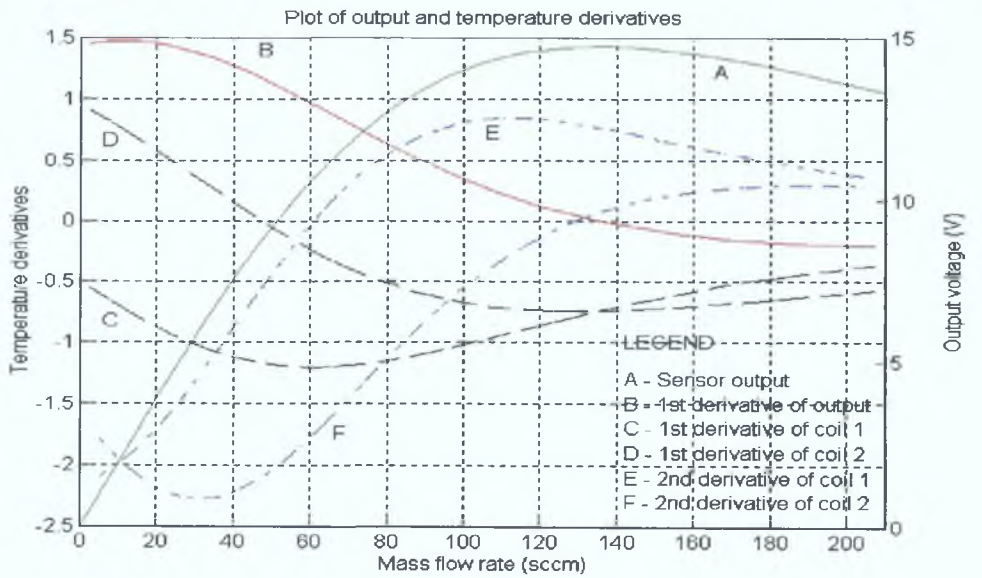

Figure 3.7b Temperature derivatives

1) Initial observations at $m = 0$ sccm

When the mass flow rate is equal to zero, the temperatures measured at both the upstream (1) and downstream (2) coils are identical since the coils are located symmetrically about the axial centre line of the sensor This results in temperature differential (ΔT) being equal to zero It can be seen that coil 1 begins to lose heat for all MFRs greater than zero, while coil 2 gains heat with the convected heat added from upstream The output graph is initially concave upwards This is more evident on inspection of *(B)* in Figure 3 7

2) • 10 sccm (Point of inflexion of output curve)

The first derivative curves *(B,C,D)* may be thought of as being proportional to heat loss by virtue of Fourier's law For increasing flow rates the average temperature of coil 1 progressively decreases with heat loss The point of inflexion in the output curve is very difficult to determine from curve A but can be recognised more easily by the intersection of the two second derivative curves *(E & F)* where the rate of change of heat loss for both coils is equal For coil 1 the rate of change of heat loss *(E)* initially decreases steadily This is in contrast to coil 2 *(F)* where it first increases Nevertheless it is initially less than coil 1 as it receives heat from it

3) >• 45 sccm and <• 60 sccm (Net heat loss in downstream coil)

At approximately 45 sccm and beyond it can be seen that there is a net heat loss in coil 2 whose temperature is at a maximum This is due to the fact that the rate of increase at which heat is being supplied by coil 1 is falling and is equal to zero at around 60 sccm At this MFR a significant point has been reached that corresponds to the limiting point of the heat transfer from the coils to the flowing gas For reduced transit times, the coils cannot supply heat to the gas at a faster rate than it is convected away Note also that this particular critical point is evident at a higher MFR for the downstream coil as its heat supply includes that of coil 1 along with its own internally generated heat

4) • 135 sccm (Downturn on output curve)

The downturn on the output curve occurs when the heat lost from both coils is identical After this point the downstream coil loses more heat than its upstream counterpart Consequently the temperature difference between the coils must decrease This turning point is the maximum design range for the sensor, as an

ambiguous output voltage that relates to two different values of MFR cannot be allowed

3.4.3 Influence of temperature on the heat input to the sensor

Equation 3 21 can be seen to consider the heat supply to be evenly distributed along the length of the sensor as a first approximation model (The constant current supply to the sensor windings (56Ω each) is 47mA) This uniformity of heat distribution will arise only if it assumed that the resistance of the coils remains constant However, from fundamental physics it is known that the resistance (R) of the windings will vary with temperature, and hence the heat input q will also vary

q may be written as $q = \frac{I^2 R(1+\alpha T)}{L} = q_0(1+\alpha T)$, where α is the temperature coefficient of resistance and with T being the temperature above T_a The temperature is constrained to be at T_a at each end of the sensor Equation 3 21 is now rewritten as

$$kA\frac{d^2T}{dX^2} - mC_p\frac{dT}{dX} = -q_0(1+\alpha T) \qquad \text{Equation 3 23}$$

The solution to this equation depends on whether the roots of the auxiliary equation of equation 3 23 given by $r_{1,2} = \frac{mC_p \pm \sqrt{(mC_p)^2 - 4kAq_0\alpha}}{2kA}$ are real or complex values

Complex values may be thought of as in the case of 2nd order underdamped linear differential equations in the time domain where high frequency ripples are added to the output

$$T(x,m) = \left(\alpha^{-1} - \frac{\alpha^{-1}\left(1-e^{r_1 L}\right)}{e^{r_2 L} - e^{r_1 L}}\right)e^{r_1 X} + \left(\frac{\alpha^{-1}\left(1-e^{r_1 L}\right)}{e^{r_2 L} - e^{r_1 L}}\right)e^{r_2 X} - \alpha^{-1} \qquad \text{(a)}$$

$$T(x,m) = e^{\mathrm{Re}(r_1)X} * \left\{\frac{1}{\alpha}\cos(\mathrm{Im}(r_1)X) + \frac{e^{-\mathrm{Re}(r_1)X} - \cos(\mathrm{Im}(r_1)L)}{\alpha \sin(\mathrm{Im}(r_1)L)}\sin(\mathrm{Im}(r_1)X)\right\} - \frac{1}{\alpha} \qquad \text{(b)}$$

Equation 3 24

Re( ) and *Im( )* denote the real and imaginary parts of the complex roots

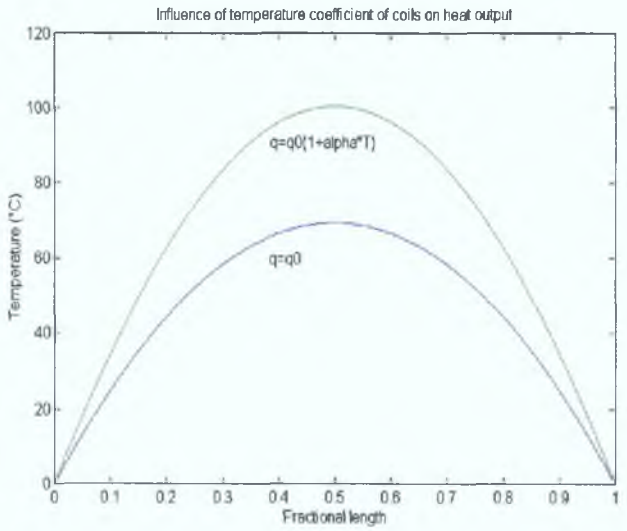

Figure 3.8 Temperature distribution for changing temperature coefficient

Equation 3.24(a) and 3.24(b) give the solution when there are real and complex roots respectively. The chosen equation depends on the parameter values used in computation.

T is plotted as a function of fractional length in Figure 3.8 for zero mass flow. It can be seen that the temperature coefficient of resistance α has a significant effect or non negligible on the output. As a result, α was taken into account for the remaining models in the thesis. Figure 3.9 shows the marked difference in the output curve. The output is greater as more heat is actually added then was taken account of in the model in section 3.4.1.

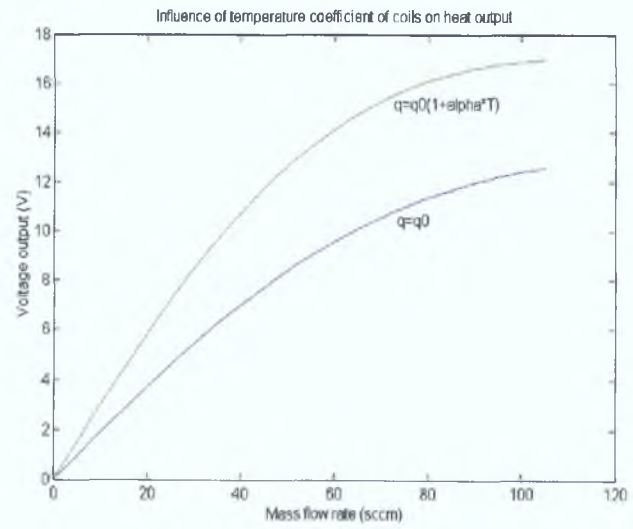

Figure 3.9 Change in output when temperature coefficient is included

3.4.4 Parabolic distribution of heat input over the length of the sensor

Since the heat supplied to the sensor is not uniform over the whole of its length, it was decided to try to approximate the heat input per unit length in a parabolic (or quadratic form) $\dot{q}(X) = aX^2 + bX + c$ as a function of axial length. This had the effect of concentrating the heat input to the centre of the sensor with no heat being added at the extremities. Figure 3.10 shows the actual heat distribution where the heat is centred on 11% of the sensor (as in Unit Instruments design) and also both constant and parabolic heat distributions. Note the total heat added in all three cases to the sensor is the same. This can be measured from the area underneath the curves.

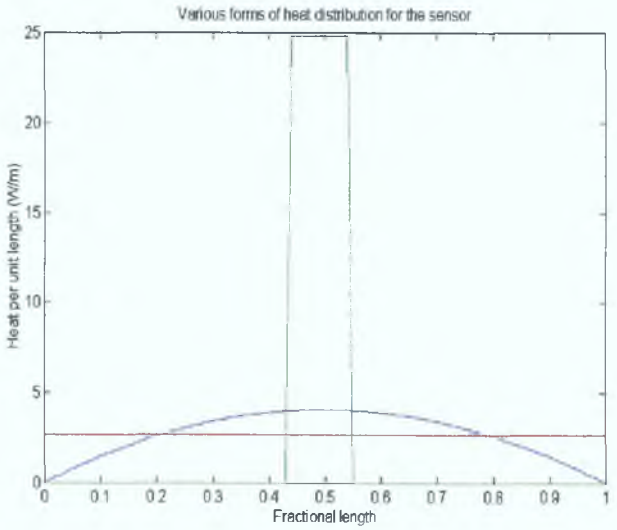

Figure 3.10 Different heat distributions along the sensor

Known points on the curve are: $\dot{q}(0) = 0$ and $\dot{q}(L) = 0$ also.

From the above points on the curve the parabolic form reduces to $\dot{q}(X) = aX^2 + aLX$.

Total heat supplied = $Q = \int_0^L (aX^2 - aLX)dx$ from which $a = -6Q/L^3$.

Therefore $\dot{q}(X) = \frac{6Q}{L^2}X - \frac{6Q}{L^3}X^2$ and the model equation may be written as :

$$\frac{d^2T}{dX^2} - \frac{\dot{m}C_p}{kA}\frac{dT}{dX} = -\dot{q}(X)\frac{1+\alpha T}{kA} \qquad \text{Equation 3.25}$$

A plot of the output is shown in Figure 3.11. This compares the sensor output for a constant versus a parabolic distribution of heat per unit length. The effect of the

parabolic distribution is to largely increase the output. Unfortunately a reduction rather than an increase in output is needed to match the model output with the rig data.

The next step was to consider heating only a central part of the sensor, which is actually the case.

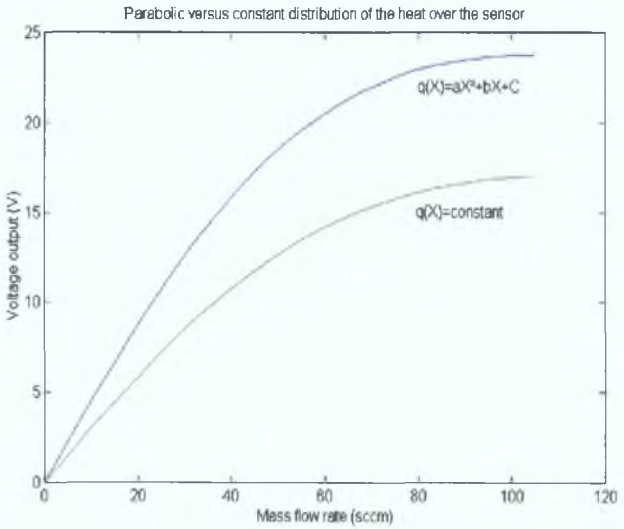

Figure 3.11 Output change for parabolic heat distribution

3.4.5 Derivation of solution for heated middle section of sensor

On examination of the sensor, it can be seen that all the heat supplied to the sensor is centred on region 2 of Figure 3.12. In regions 1 and 3, the heat input is equal to zero. For all three regions, equation 3.23 applies. h is a variable parameter upon which the heat input per unit length, $\dot{q}$,depends. ($\dot{q} = I^2 R(1+\alpha T)/2h$)

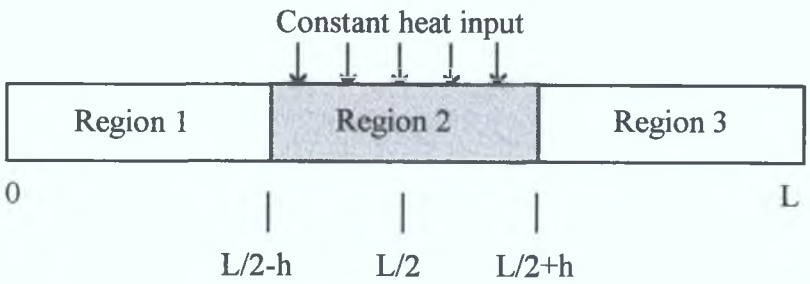

Figure 3.12 Sensor divided into three axial regions

The form of the solution for the three regions is as follows:

Region 1: $T = C_1\left(e^{\lambda X} - 1\right)$ Equation 3.26(a)

Region 2: $T = C_2 e^{r_1 X} + C_3 e^{r_{21} X} - \frac{1}{\alpha}$ Equation 3.26(b)

Region 3: $T = C_4\left(e^{\lambda X} - e^{\lambda L}\right)$ Equation 3.26(c)

It can be shown by Taylor series expansions that equations 3.26(a) and 3.26(c) reduce to a linear form as $\dot{m}$ goes to zero, while equation 3.26(b) reduces to a quadratic as would be expected. In matrix form, equating the temperatures and the derivatives at the regional boundary points, the following expression is arrived at:

$$\begin{bmatrix} e^{\lambda\left(\frac{L}{2}-h\right)} - 1 & -e^{r_1\left(\frac{L}{2}-h\right)} & -e^{r_2\left(\frac{L}{2}-h\right)} & 0 \\ 0 & -e^{r_1\left(\frac{L}{2}+h\right)} & -e^{r_2\left(\frac{L}{2}+h\right)} & -e^{\lambda\left(\frac{L}{2}+h\right)} - e^{\lambda L} \\ \lambda e^{\lambda\left(\frac{L}{2}-h\right)} & -r_1 e^{r_1\left(\frac{L}{2}-h\right)} & -r_2 e^{r_2\left(\frac{L}{2}-h\right)} & 0 \\ 0 & -r_1 e^{r_1\left(\frac{L}{2}+h\right)} & -r_2 e^{r_2\left(\frac{L}{2}+h\right)} & \lambda e^{\lambda\left(\frac{L}{2}+h\right)} \end{bmatrix} \begin{bmatrix} C_1 \\ C_2 \\ C_3 \\ C_4 \end{bmatrix} = \begin{bmatrix} -\frac{1}{\alpha} \\ -\frac{1}{\alpha} \\ 0 \\ 0 \end{bmatrix}$$

Equation 3.27

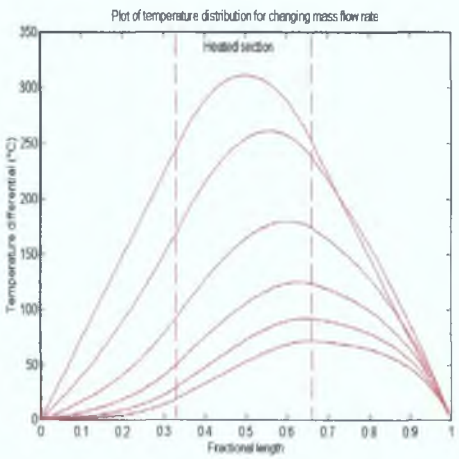

Figure 3.13 Temperature distribution for changing mass flow rate

This matrix system can be easily solved using MATLAB®, a mathematical package, to obtain the desired coefficients [42]. A MATLAB® script file was written to calculate the matrix values values for variations in both mass flow rate and the length of the middle section. Using these values, the temperature distribution values may be computed, from which the average temperature in the coils is calculated by integrating the temperature profile over the coils range. Figure 3.13 shows the temperature profile when the sensor is heated only in the middle third for varying mass flow rates.

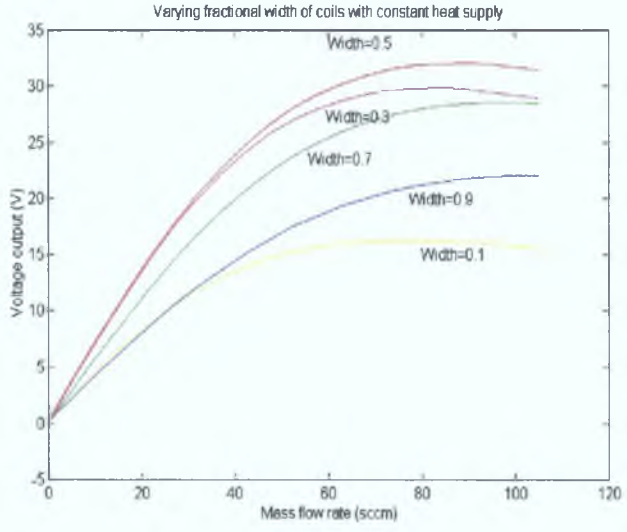

Figure 3.14 Output curve for variable coils' length

Figure 3.14 shows the change in the output curve for changes in the length of the heated centre region (expressed as a fractional length). It can be seen that the sensor output has maximum sensitivity when half the length of the sensor is heated. It is not understood why the manufacturers of the sensor heat only 11% of the sensor length bearing this fact in mind. The operating range of the sensor (~100sccm) is not relevant since only ~10sccm of a sensor range is ever used and all the nonlinearity is effectively negated by the associated linearising circuitry. This fact was ascertained in analysing some Unit Instruments meters and calculating the flow through the sensor for the maximum flow of each meter.

3.4.6 Effect of having a small gap between the coils

There exists on the actual sensor a small gap of approximately 1mm between the heating coils. The model was changed to accommodate this fact. It was concluded that the effect of this slight gap on the sensor output was negligible.

3.4.7 Effect of model parameter tolerance on output

There are six parameters associated with the model to this point, each of which will be examined individually to see its effect on the meters output.

1) Cross sectional area(CSA) of the sensor

This value is dependent on the internal and external diameters of the sensor. The sensor measurements are quoted as an internal diameter Di = 0.031"+0.002" (0.7874mm+0.0508mm), and a wall thickness W = 0.008"±0.0008" (0.2032mm+0.02032mm) [29]. From these measurements table 3.1 may be constructed showing the variation of the cross sectional area of the sensor expressed as a percentage of the nominal value for different combinations.

It can be seen from the table that there is a 40% deviation between the minimum and maximum values, the effect of which is shown in Figure 3.15. Clearly the accuracy quoted is not adequate for modelling purposes.

An accurate measurement of the sensor was taken using a micrometer and insertion-type gauges. Table 3.2 shows a significant reduction of the error associated with the specified values. The output bounds are also shown in Figure 3.15 for comparative purposes.

Table 3.1 Variation of cross sectional area using the given tolerances

	Inner diameter 0.001" (0.0254mm)	Wall thickness 0.001" (0.0254mm)	Outer diameter 0.001" (0.0254mm)	Area/(Nom. area) %
Nominal	31	8	47	100
	31	7.2	45.4	88.2
	31	8.8	48.6	112.3
	33	7.2	45.4	77.9
	33	8.8	50.6	117.9

Table 3.2 Variation of cross sectional area using measured values

	Inner diameter (mm)	Outer diameter (mm)	Area/(Measured. Area) %
Measured	0.81±0.01	1.21±0.01	100
Min. area	0.82	1.21	98.0
Max. area	0.80	1.22	105.0

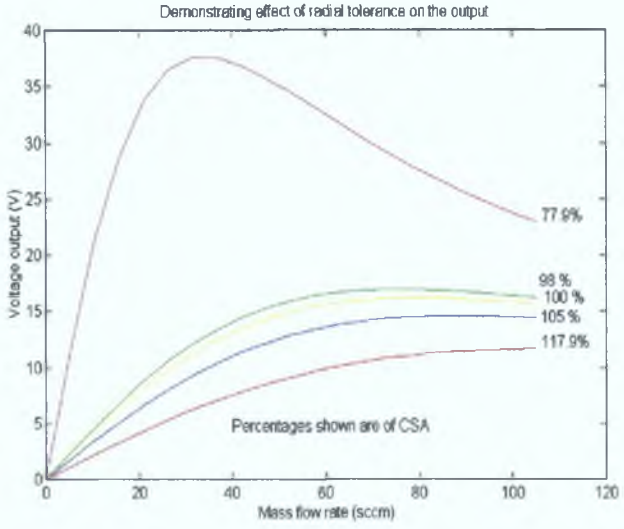

Figure 3.15 Effect of radial tolerance on the output

The change in the output is as expected. Radial tolerances have such a large effect because the error in both the internal and external radii are squared and accumulated. As the cross sectional area is reduced, it is possible for more heat to be transferred to the gas to produce a greater temperature differential between coils.

2) Length of the sensor

The length of the sensor is given as 3.5" + 0.01" (88.9 mm + 0.254 mm). There is a negligible effect on the model output when the tolerance value is added. This is to be expected since the tolerance corresponds to only a 0.29% measurement error. It is a very low tolerance compared with the 10% specified for the wall thickness. The difficulty in manufacture lies in trying to produce a high aspect ratio sensor with small diameter.

3) Constant current input into coils

Changes in the constant heat supply into the coils are directly proportional to the sensor output to a first approximation. This can be witnessed alternatively by consideration of equation 3.22. Thus a square law $\left(I^2 \propto V_{out}\right)$ relates the constant current input supply to the sensor output. By changing the model's coils width, it was seen that the former statement remains true.

4) Thermal conductivity of the sensor

The effect of a one percent change in the thermal conductivity is shown in Figure 3.16. The need for an accurate value of thermal conductivity is thus illustrated for all models.

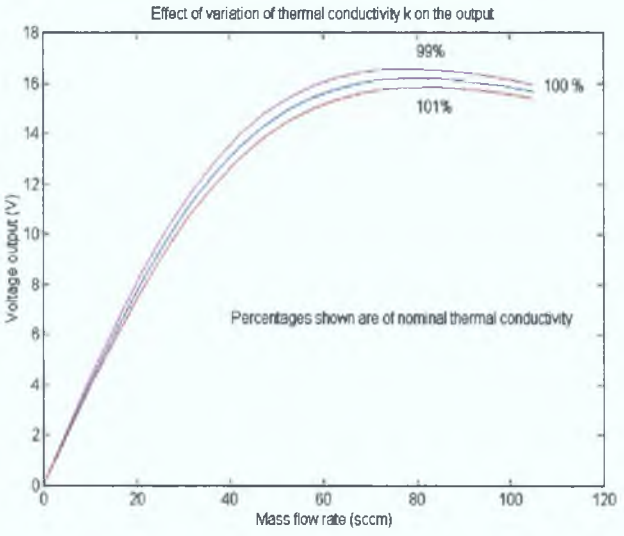

Figure 3.16 Effect of thermal conductivity

5) Specific heat capacity of the gas

The effect of a one percent change in the specific heat capacity is shown in Figure 3.17. By comparison with the previous parameters discussed, the model is relatively insensitive to variations in this particular one. The value of this parameter is quoted with 4 significant figures with a change in the least significant figure corresponding only to a 0.1 % variation.

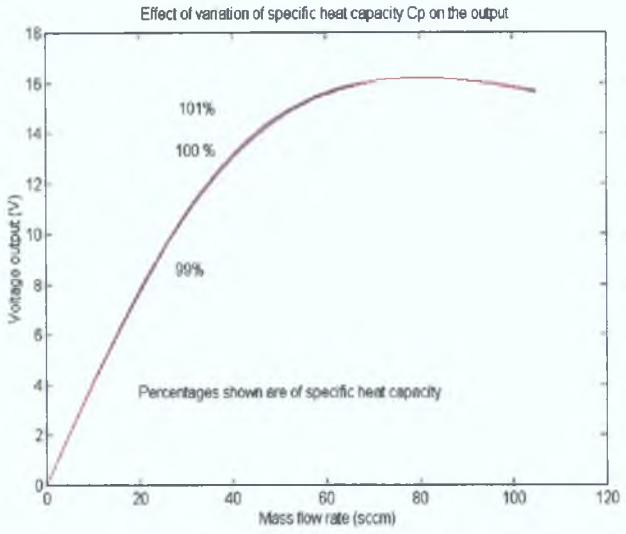

Figure 3.17 Effect of specific heat capacity

6) Thermal coefficient of the coils

Likewise as for the thermal conductivity and the specific heat capacity, the model was subjected to a one percent change in the thermal coefficient of the coils in order to view its effect which is shown in Figure 3.18.

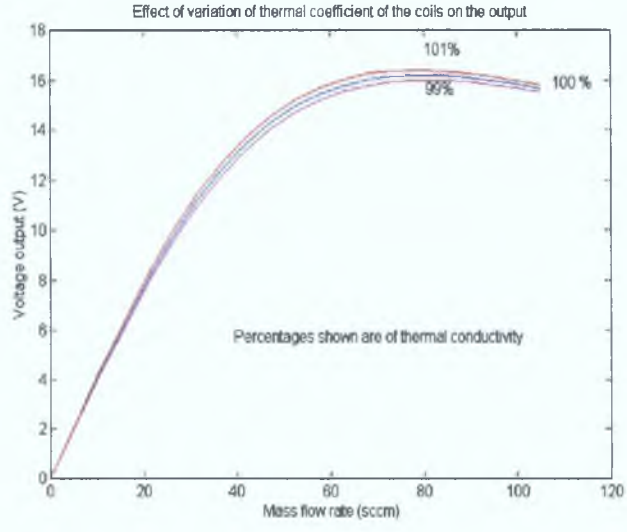

Figure 3.18 Effect of the coils' thermal conductivity

The value of this parameter is quoted to 4 decimal places with a change in the least significant digit corresponding to a 1.5% variation.

7) Ambient temperature of meter surroundings and gas.

Ambient temperature changes have a noticeable effect on the output of the model. This can be attributed entirely to the resistance of the coils and consequently the heat added. If the resistance of the coils, R, is examined, it can be seen that $R = R_{AMBIENT}(1+\alpha(T - T_{AMBIENT}))$. By assuming that the ambient temperature in the models is 0°C, the temperature rise (or fall) above ambient is only of concern. The same effect is recognisable in the actual sensor operation. No further mention will be made of this factor in the following chapters as no data was logged to validate the model. Its effect was merely noted. Figure 3.19 shows the change in output for a similar sensor for which radial and axial measurements were not available.

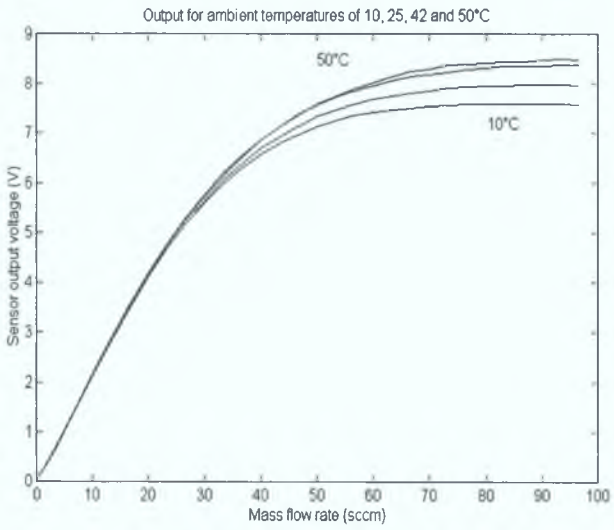

Figure 3.19 Effect of ambient temperature on the output

3.5 Summary

This chapter described the one-dimensional (1D) modelling of the sensor along with a bypass model. Inclusion of the derivation of the bridge output voltage as a function of differential temperature allows a complete simulation of the mass flow meter. The model output gained reproduces the form of published work and a comprehensive explanation is provided for the shape of the output curve. The linearity of the bypass arrangement was validated in a separate model that showed that the sensor flow to

bypass flow can be taken to be constant (with negligible error) for changing mass flow rates However the magnitude of the output for the first model is much higher than expected when it is compared to experimental data

Each of the alterations that were made to the model with regard to the heat distribution over the sensor drastically changed its output as expected These are not merely scaling changes as, although the general curve characteristic is preserved, its maximum occurs at different mass flow rates Distributing the heat in a parabolic fashion was not considered beneficial to the model When reducing the fractional heated length to 11% of the sensor to further refine the model, the magnitude of the output reduces considerably in agreement with experimental data However when taking into account the thermal coefficient of resistance of the coils, the magnitude is increased

It has been observed that the model is sensitive to the different parameter tolerances to considerably varying degrees Radial tolerances are the most critical model parameter of all Perhaps if the sensor manufacturers specified a reduced tolerance, they would have no need to individually calibrate sensors for mass flow meters The model is also particularly sensitive to variations of the thermal conductivity of the sensor and insensitive by comparison to variation of the specific heat capacity and the thermal coefficient of the coils Variation in the quantity of heat added to the sensor manifests itself as merely a scaling of the output

The only drawback to the 1D models developed is that the effect of the thermal conductivity of the gas or the heat loss to the meters surroundings cannot be seen The examination of these effects are presented in the following chapter In this chapter, the specific heat capacity was the only gas property used to characterise and differentiate each of the various gases

CHAPTER 4

TWO-DIMENSIONAL (2-D) MODELLING

4.1 Introduction :

This chapter extends the models of the previous chapter for the mass flow rate sensor to three dimensional space. Since the sensor is axially symmetric, all references to the polar angle of the cylindrical coordinate system in the heat equations can be removed, and the temperature field may then be considered two dimensional. All equations are independent of time so as to derive the steady-state response.

The resulting equations from the above process yields a system of elliptic partial differential equations (PDEs), and their associated boundary conditions. Finite differencing is utilised to provide a solution to this system, followed by numerical integration to find the average temperature in the coils.

Current mathematical software capable of obtaining a solution is listed along with an explanation of the code used.

4.2 Derivation of temperature distribution equations :

Figure 4.1 below shows the mass flow sensor and its surrounding layers. The sensor

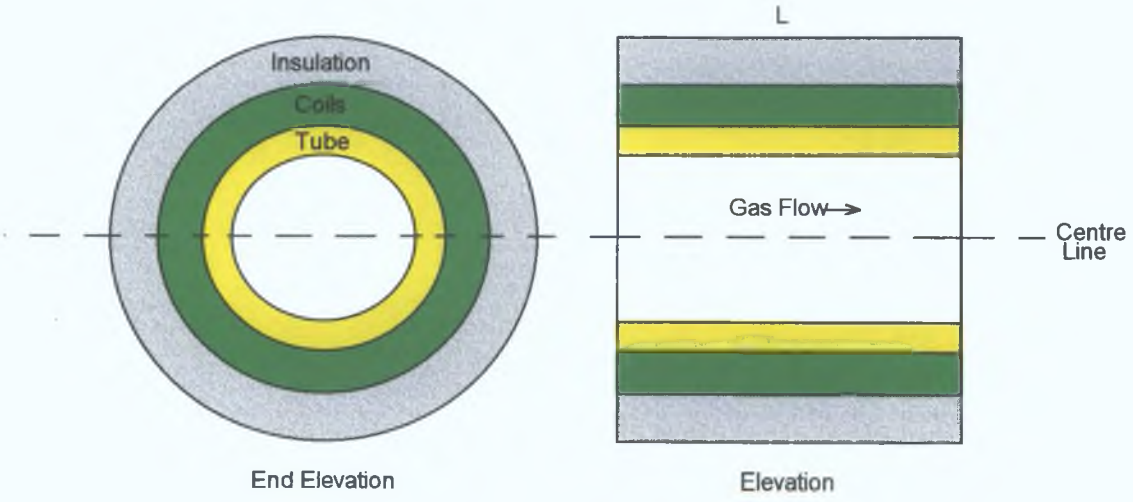

Figure 4.1 Layer structure of the sensor

tube is enveloped by the heating coils and by a further layer of insulation. Figure 4.2 shows an enlarged view of half the elevation of Figure 4.1. It consists of a number of subsystems for which the temperature distribution must be calculated. Thermal resistances are shown which exist at the boundaries of each of the subsystems. They are also present within to indicate the resistance to heat flow in both the axial and radial directions.

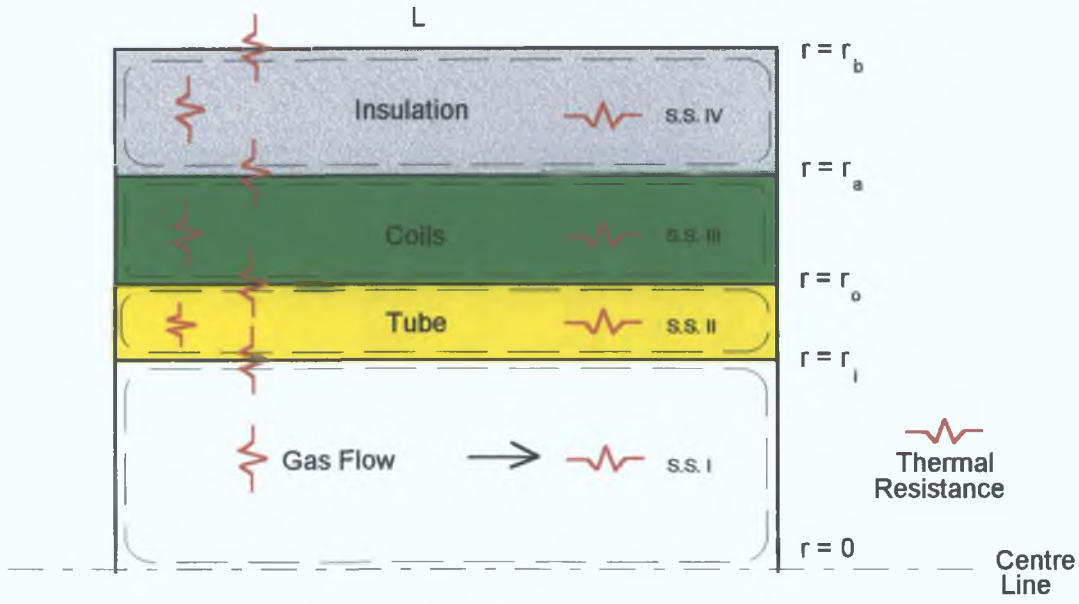

Figure 4.2 Thermal resistances within the sensor

Heat transfer into and out of the system occurs by a combination of conduction, convection and radiation. Conduction occurs due to the influence of a temperature gradient between molecules. In a flowing streamlined fluid, convection is the dominant heat transfer method present. Heat is also transferred simultaneously by molecular conduction to a lesser extent. On the outer boundary, heat is dissipated by a combination of natural convection and radiation. In this case heat loss due to radiation is negligible compared to the convection present and will not need to be included in the final set of equations.

An annular element of length dx is considered for each subsystem. The inner and outer radii of the annular element are r and $r+dr$ respectively. See Figure 4.3.
Heat may flow into the annular element by each of three methods:

1) Conduction radially,

2) Conduction axially,

3) Convection through the gas.

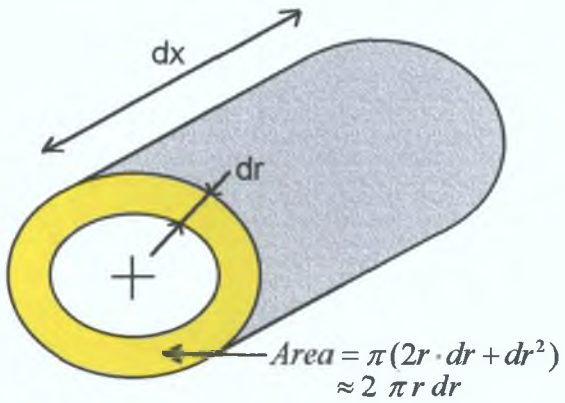

Figure 4.3 Annular element of the sensor

Consider first subsystem 1 (S.S. I) inside the tube from Figure 4.2. Equations are derived using a similar procedure to [34].

Heat conducted into the annular element in the radial direction is

$$dq_r = -k_G 2\pi r dx \left.\frac{\partial T_I}{\partial r}\right|_r \qquad \text{Equation 4.1}$$

where q is heat conducted, k_G is the thermal conductivity of the gas and T_I is the temperature in S.S. 1.

Heat conducted out of the annular element in the radial element is

$$dq_{r+dr} = -k_G 2\pi (r+dr) dx \left.\frac{\partial T_I}{\partial r}\right|_{r+dr} \qquad \text{Equation 4.2}$$

By Taylor's Theorem

$$\left.\frac{\partial T_I}{\partial r}\right|_{r+dr} = \left(\frac{\partial T_I}{\partial r} + dr\frac{\partial^2 T_I}{\partial r^2} + \cdots\right) \qquad \text{Equation 4.3}$$

So net heat conducted in radially is

$$2\pi r k_G \left(\frac{\partial T_I}{\partial r} + r\frac{\partial^2 T_I}{\partial r^2}\right) dx dr \qquad \text{Equation 4.4}$$

Similarly heat conducted in axially is

$$2\pi r k_G \frac{\partial T_I}{\partial x^2} dx dr \qquad \text{Equation 4.5}$$

Convection into the element is

$$q_x = 2\pi r \cdot dr \cdot u(r)\rho C_p T_I \qquad \text{Equation 4.6}$$

where u, ρ and C_p are the velocity, density and specific heat capacity of the gas respectively. Convection out of the element is:

$$q_{x+dx} = 2\pi r \cdot dr \cdot u(r)\rho C_p \left(T_I + \frac{\partial T_I}{\partial x} dx \right) \qquad \text{Equation 4.7}$$

Net heat convected out is

$$2\pi r \cdot dr \cdot u(r)\rho C_p \frac{\partial T_I}{\partial x} dx \qquad \text{Equation 4.8}$$

At equilibrium,

Net convection out = net conduction in radially + net conduction in axially

$$2\pi r\, dr\, u(r)\, \rho C_p \frac{\partial T_I}{\partial x} dx = 2\pi r k_G \left(\frac{\partial T_I}{\partial r} + r \frac{\partial^2 T_I}{\partial r^2} \right) dx\, dr + 2\pi r k_G \frac{\partial^2 T_I}{\partial x^2} dx\, dr$$

Equation 4.9

$$u(r)\rho C_p \frac{\partial T_I}{\partial x} = k_G \left(\frac{1}{r} \frac{\partial T_I}{\partial r} + \frac{\partial^2 T_I}{\partial r^2} \right) + k_G \frac{\partial^2 T_I}{\partial x^2} \qquad \text{Equation 4.10}$$

$$k_G \frac{\partial^2 T_I}{\partial x^2} + k_G \frac{\partial^2 T_I}{\partial r^2} + \frac{k_G}{r} \frac{\partial T_I}{\partial r} - u(r)\rho C_p \frac{\partial T_I}{\partial x} = 0 \qquad \text{Equation 4.11}$$

$$\frac{\partial^2 T_I}{\partial x^2} + \frac{\partial^2 T_I}{\partial r^2} + \frac{1}{r} \frac{\partial T_I}{\partial r} - \frac{\dot{m}(r) C_p}{k_G A_I} \frac{\partial T_I}{\partial x} = 0 \qquad \text{Equation 4.12}$$

where $A_I = \pi r_i^2$ and $\dot{m}(r) = A_I \rho u(r)$ Equation 4.13

It is important to note that the mass flow rate $\dot{m}$ is a function of the radial length of the pipe. The output value for mass flow rate through the sensor, $\dot{m}_B$, is a bulk stream value for the entire cross section of the pipe and is related to the bulk velocity u_B by the formula $\dot{m}_B = \rho A u_B$. The velocity and mass flow rate as a function of the radius can be shown to be of the following parabolic forms if the gas has a smooth laminar flow [5]:

$$u(r) = 2u_B \left[1 - \left(\frac{r}{r_i} \right)^2 \right] \text{ and } \dot{m}(r) = 2\dot{m}_B \left[1 - \left(\frac{r}{r_i} \right)^2 \right] \qquad \text{Equation 4.14}$$

Equation 4 12 complements the equation derived in [35] for flow in a circular tube under conditions of steady laminar flow with low velocities, no concentration gradients, negligible pressure gradient, no source functions, and with symmetric heat transfer and hydrodynamically fully developed flow present The equation can be seen to be in the cylindrical orthogonal coordinate system as this is the most suitable to use due to the geometry of the sensor

By a similar procedure, expressions for subsystems 2, 3, and 4 may be obtained and are recognisable as Laplace's and Poisson's equations

$$\frac{\partial^2 T_{II}}{\partial x^2}+\frac{\partial^2 T_{II}}{\partial r^2}+\frac{1}{r}\frac{\partial T_{II}}{\partial r}=\nabla^2 T_{II}(x,r)=0 \qquad \text{Equation 4 15}$$

$$\frac{\partial^2 T_{III}}{\partial x^2}+\frac{\partial^2 T_{III}}{\partial r^2}+\frac{1}{r}\frac{\partial T_{III}}{\partial r}=\nabla^2 T(x,r)=-\frac{-q(1+\alpha T_{III})}{k_C}=-\frac{-q(1+\alpha T_{III})}{k_C}$$

Equation 4 16

where $A_2=\pi\left(r_a^{\,2}-r_o^{\,2}\right)$, k_C is the thermal conductivity of the coils and q and q are heat input per unit length and per unit volume respectively

$$\frac{\partial^2 T_{IV}}{\partial x^2}+\frac{\partial^2 T_{IV}}{\partial r^2}+\frac{1}{r}\frac{\partial T_{IV}}{\partial r}=\nabla^2 T_{IV}=0 \qquad \text{Equation 4 17}$$

4.2.1 Boundary conditions

Boundary conditions must be expressed for a complete mathematical formulation of the composite system

The temperature at the left and rightmost boundary for each subsystem is taken to be at ambient temperature Mathematically this may be expressed as

$T_J\left(x\in\{0,L\},r\right)=0$, J (Regions I to IV) Equation 4 18

$$\left.\frac{\partial T_J}{\partial r}\right|_{r=0}=0 \qquad \text{Equation 4 19}$$

This is chosen so that the temperature on the centre line remains finite A more intuitive understanding can be gained by realising that the centre line must be insulated for it to be a line of symmetry

Energy balance at boundaries (Fourier's Law)

At the boundary between the pipe and the gas the following relationship applies

$$-k_P \left.\frac{\partial T_{II}}{\partial r}\right|_{r=r_i} = h_1 \left(T_{II}|_{r=r_i} - T_B\right)_{average} \qquad \text{Equation 4 20}$$

where the bulk temperature T_B, is the average temperature of the gas along the length of the sensor and is a function of axial length h_1 is the convection heat transfer coefficient at the sensor-gas interface

At the boundary between the pipe and the coils

$$k_P \left.\frac{\partial T_{II}}{\partial r}\right|_{r=r_o} = k_C \left.\frac{\partial T_{III}}{\partial r}\right|_{r=r_o} \qquad \text{Equation 4 21}$$

At the boundary between the coils and the insulation

$$k_C \left.\frac{\partial T_{III}}{\partial r}\right|_{r=r_a} = k_I \left.\frac{\partial T_{IV}}{\partial r}\right|_{r=r_a} \qquad \text{Equation 4 22}$$

k_P, k_C and k_I are the thermal conductivity of the pipe, coils, and insulation respectively

A perfect contact between the surfaces requires the absence of gases or vacant spaces caused by those blowholes, bubbles, or rough surfaces which are very likely to be present when two solids are brought together Traces of poorly conducting materials such as oxide films will cause abrupt drops in the temperature

If the thermal contact resistances between the subsystems is not equal to zero, the temperatures at their boundaries cannot be equated A different interfacial boundary condition then applies and a thermal contact coefficient (h_{c1} and h_{c2}) must be sought

$$T_{III}\big|_{r=r_a} = T_{II}\big|_{r=r_a} + \frac{k_P}{h_{c1}} \frac{\partial T_{II}}{\partial r}\bigg|_{r=r_a}$$ Equation 4.23

$$T_{III}\big|_{r=r_a} = T_{IV}\big|_{r=r_a} + \frac{k_C}{h_{c2}} \frac{\partial T_{III}}{\partial r}\bigg|_{r=r_a}$$ Equation 4.24

At the external boundary, any heat lost is naturally convected away by air at ambient temperature. This assumes that the radiation of heat from the insulation, given its quality, is negligible as stated earlier and this is desirable for obtaining a solution. The introduction of a radiation term would involve temperature terms to the fourth power (from the Stefan-Boltzmann Law), and would give an undesirable non-linear system of equations to solve as an unwieldy iterative approach would be necessary.
So the external boundary condition is taken as:

$$-k_I \frac{\partial T_{IV}}{\partial r}\bigg|_{r=r_b} = h_2\left(T_{IV}\big|_{r=r_b} - T_\infty\right)$$ Equation 4.25

where h_2 is the convection heat transfer coefficient at the insulation-air interface. T_∞ is the ambient temperature of the surroundings.

4.3 Solution methods :

In the case where the boundaries of a region are regular, many methods exist to obtain an analytical solution to partial differential equations. These techniques include separation of variables (product solution), Laplace and integral transforms. In addition approximate analytical, numerical, analogical, and graphical methods also exist.

For a single body system, separation of variables is the most applicable method where the heat transfer problem is in more than one dimensional. Unfortunately for a composite system such as the MFM, it is too cumbersome to use any analytical methods. Small changes to the system for improved models would prove very time

consuming It is with this in mind that attention was drawn towards the numerical techniques available today

One may employ a numerical approximation method such as the Finite Difference (FD), the Finite Element (FE), or the Boundary Element (BE) Method to solve the governing equations

The classical numerical treatment for partial differential equations is the Finite Difference Method where the solution domain is approximated by a grid of uniformly spaced nodes At each node, the governing differential equation is approximated by an algebraic expression that references adjacent grid points A system of equations is obtained and solved for each value In the Finite Element Method, the solution domain is discretised into a number of uniform or non-uniform finite elements that are connected via nodes The change of the dependent variable with regard to location is approximated within each element by an interpolation function The interpolation function is defined relative to the values of the variable at the nodes associated with each element The original boundary value problem is then replaced by an equivalent integral formulation that is reformulated into a matrix equation that is subsequently solved for the unknown variable Boundary Element Methods are seldom used

4.3.1 Available software

Many thermal software packages are currently available for the solution of partial differential equation type problems Most of them are written in the area of computational fluid dynamics and some are available as shareware or freeware on the World Wide Web (WWW) However these shareware and freeware programmes are generally very specialised and are not maintained by the authors For the most part, the packages are available commercially Three such packages are briefly mentioned there are many more

1) HEATING

"HEATING is a general-purpose, conduction, heat transfer program written and maintained by the Heat Transfer and Fluid Flow Group (HTFFG) [36] HEATING is written in FORTRAN 77 and can solve steady-state and/or transient heat conduction problems in one-, two-, or three-dimensional Cartesian, cylindrical, or spherical coordinates A model may include multiple materials, and the thermal conductivity, density, and specific heat of each material may be both time- and temperature-dependent The boundary conditions, which may be surface-to-environment or surface-to-surface, may be specified temperatures or any combination of prescribed heat flux, forced convection, natural convection, and radiation The boundary condition parameters may be time- and/or temperature-dependent General graybody radiation problems may be modelled with user-defined factors for radiant exchange The mesh spacing may be variable along each axis
Three steady-state solution techniques are available Transient problems may be solved using any one of several finite-difference schemes Crank-Nicolson implicit, Classical Implicit Procedure (CIP), Classical Explicit Procedure (CEP), or Levy explicit method (which for some circumstances allows a time step greater than the CEP stability criterion) This package was rejected for use because of its high price

2) *SINDA/FLUINT* (Systems Improved Numerical Differencing Analyzer with Fluid Integrator) is available for a wide variety of platforms [37] This program was originally developed in the 1960s by Chyrsler, TRW and the NASA Johnson Space Center It determines the solution of an analogous RC network to the specified system of equations The thermal networks can be modelled in a infinite number of ways according to engineering approximations The engineer can vary either the spatial resolution (number of elements used) or the temporal resolution (type of elements used) This package also was rejected for use because of its high price

3) *The Partial Differential Equation Toolbox*

The Partial Differential Equation (PDE) Toolbox is used in conjunction with the MATLAB technical computing environment [38] It contains powerful and flexible

tools for the study and solution of PDEs in two-space dimensions (2-D) and time Finite Element Methods (FEM) are utilised by the toolbox The toolbox also provides automatic and adaptive meshing capabilities and solves the resulting system of equations using MATLAB's proven sparse matrix solver (\) and a state-of-the-art stiff solver from the Ordinary Differential Equations Suite

The toolbox has been designed to intuitively follow the six steps associated with the PDE solution process using the finite element method The steps (and corresponding toolbox modes) are geometry definition (draw mode), specification of boundary conditions (boundary condition mode), selection of PDE coefficients that define the problem (PDE mode), finite element discretization (mesh mode), specification of initial conditions and solution of the PDE (solve mode), and postprocessing of the solution (plot mode) Unfortunately this package was not commercially available when needed as it would have proved to be a cost effective solution

4.4 Discretisation of temperature distribution equations:

Since the above equations and their associated boundary equations are sufficiently complex to preclude the use of simple solution techniques, one must turn to numerical methods to obtain the required solution Figure 4 4 shows a two-dimensional representation of an element within one of the subsystems

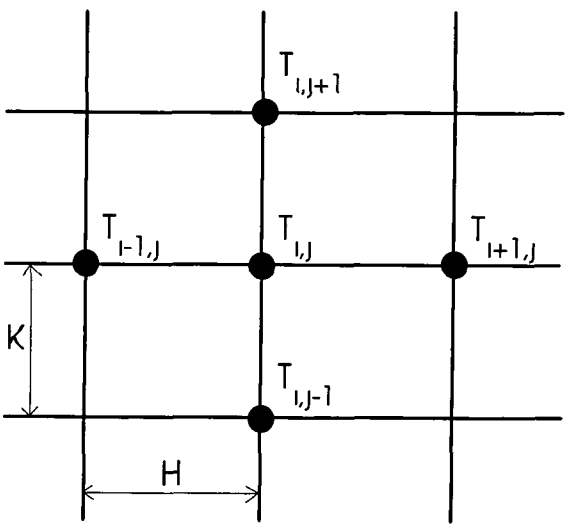

Figure 4.4 Rectangular Grid

Using the 5-Point formula the discretisations in equation 4 26 are used to approximate the partial differential equations Forward difference has been used to calculate the first derivatives, as it may lead to a more diagonally dominant matrix for those problems where the coefficients of the first derivatives are significantly larger than those of the second derivatives [39]

$$\frac{\partial^2 T}{\partial x^2}=\frac{1}{H^2}\left(T_{i+1\,j}-2T_{i,j}+T_{i-1\,j}\right) \qquad \frac{\partial^2 T}{\partial r^2}=\frac{1}{K^2}\left(T_{i,j+1}-2T_{i\,j}+T_{i,j-1}\right)$$

$$\frac{\partial T}{\partial x}=\frac{1}{H}\left(T_{i+1\,j}-T_{i,j}\right) \qquad \frac{\partial T}{\partial r}=\frac{1}{K}\left(T_{i\,j+1}-T_{i,j}\right)$$

Equation 4 26

4.4.1 Subsystem I

From equation 4 12 one gets the following using the discretisations in equation 4 26

$$\frac{\left(T_{i-1\,j}-2T_{i\,j}+T_{i+1\,j}\right)}{H^2}+\frac{\left(T_{i,j-1}-2T_{i\,j}+T_{i\,j+1}\right)}{K_I^{\,2}}+\frac{T_{i\,j+1}-T_{i\,j}}{r_j K_I}-\frac{m_j C_p}{k_G A_1}\left(T_{i+1\,j}-T_{i\,j}\right)=0$$

Equation 4 27

$$T_{i,j}\left(-\frac{2}{H^2}-\frac{2}{K_I^{\,2}}-\frac{1}{r_j K_I}+\frac{m_j c_p}{k_G A_1 H}\right)+T_{i-1,j}\left(\frac{1}{H^2}\right)+T_{i+1,j}\left(\frac{1}{H^2}-\frac{m_j C_p}{k_G A_1 H}\right)$$
$$+T_{i,j-1}\left(\frac{1}{K_I^{\,2}}\right)+T_{i,j+1}\left(\frac{1}{K_I^{\,2}}+\frac{1}{r_j K_I}\right)=0$$

Equation 4 28

4.4.2 Subsystem II

$$T_{i\,j}\left(-\frac{2}{H^2}-\frac{2}{K_{II}^{\,2}}-\frac{1}{r_j K_{II}}\right)+T_{i-1\,j}\left(\frac{1}{H^2}\right)+T_{i+1\,j}\left(\frac{1}{H^2}\right)+T_{i\,j-1}\left(\frac{1}{K_{II}^{\,2}}\right)+T_{i\,j+1}\left(\frac{1}{K_{II}^{\,2}}+\frac{1}{r_j K_{II}}\right)=0$$

Equation 4 29

4.4.3 Subsystem III

$$T_{i,j}\left(-\frac{2}{H^2}-\frac{2}{K_{III}^{\,2}}-\frac{1}{r_j K_{III}}\right)+T_{i-1,j}\left(\frac{1}{H^2}\right)+T_{i+1,j}\left(\frac{1}{H^2}\right)$$
$$+T_{i\,j-1}\left(\frac{1}{K_{III}^{\,2}}\right)+T_{i\,j+1}\left(\frac{1}{K_{III}^{\,2}}+\frac{1}{r_j K_{III}}\right)=\frac{-q\left(1+\alpha T_{i\,j}\right)}{k_c}$$

Equation 4 30

Note that again the heat input per unit volume is dependent on temperature for the coils

4.4.4 Subsystem IV

$$T_{i,j}\left(-\frac{2}{H^2}-\frac{2}{K_{IV}{}^2}-\frac{1}{r_j K_{IV}}\right)+T_{i-1\,j}\left(\frac{1}{H^2}\right)+T_{i+1\,j}\left(\frac{1}{H^2}\right)+T_{i\,j-1}\left(\frac{1}{K_{IV}{}^2}\right)+T_{i\,j+1}\left(\frac{1}{K_{IV}{}^2}+\frac{1}{r_j K_{IV}}\right)=0$$

Equation 4 31

K_I, K_{II}, K_{III} and K_{IV} refer to the radial grid spacings in the different subsystems

Each subsystem is initially divided into nine grid spaces for which the temperature at all the internal nodes is to be calculated Figure 4 5 shows the interconnection and labelling of all the nodes The temperature along the left and right hand sides is the temperature of the unheated gas, and is assumed to be at ambient temperature

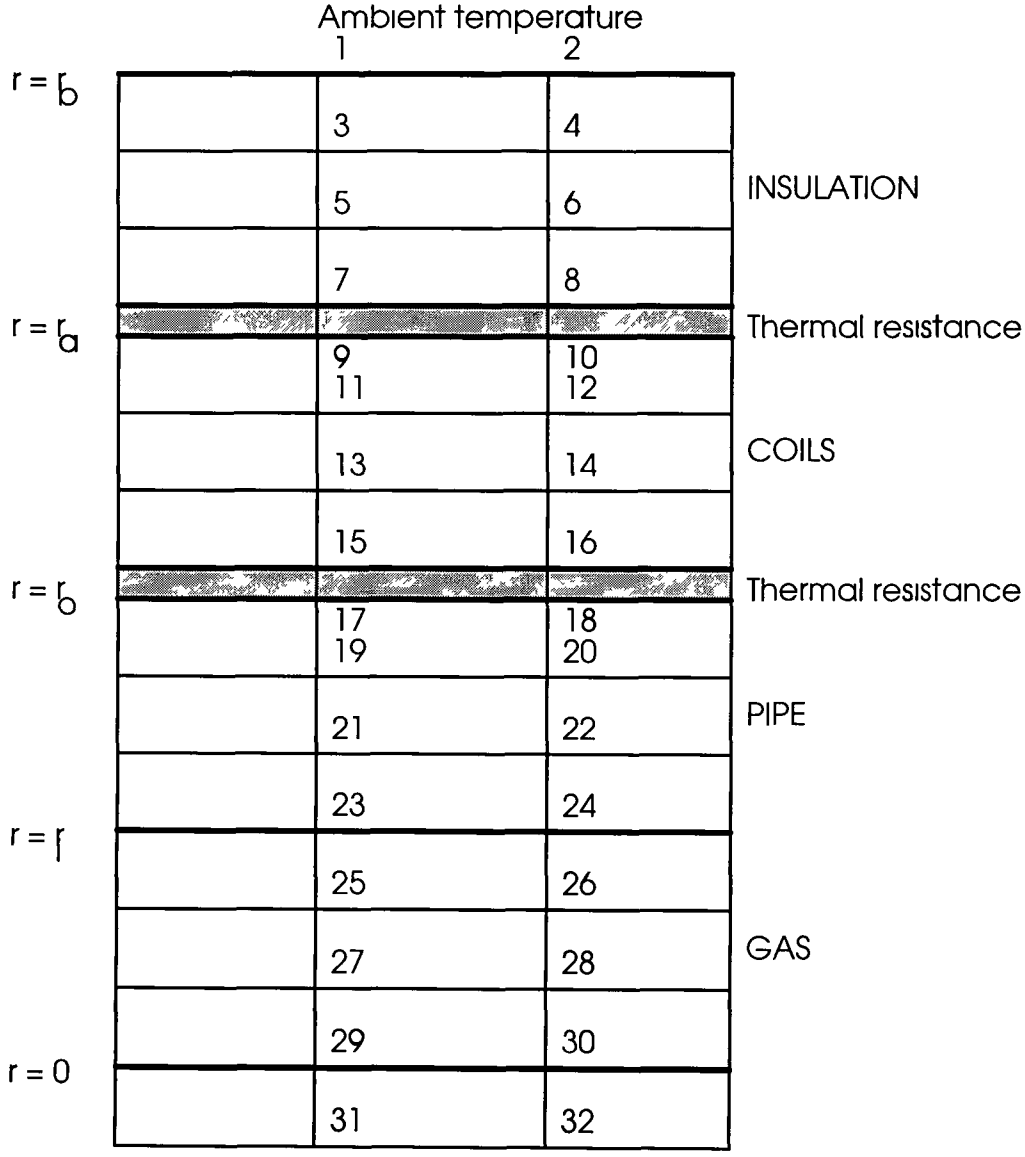

Figure 4.5 Finite difference representation of problem

Since there are thermal contact resistances between the insulation and coils, and the coils and the pipe, there will be a temperature drop at the boundaries Consequently there are separate nodes at each side of the boundaries The result of using this finite difference technique is that there will be 32 algebraic equations for each of the 32 nodes in the system These replace the partial differential equations and their associated boundary conditions A matrix form of these equations may be constructed, from which one may use standard techniques such as Gaussian elimination to solve for the nodal temperatures

However the procedure needs to be generalised to obtain temperatures for an increasing number of nodes The more nodes taken, the closer the approximation of the difference equation will be to the partial differential equation As a result the forementioned matrix inversion techniques are not well-suited for obtaining a solution An iteration technique such as Gauss-Siedel may be used [40][41] This is a more efficient method of solution than a direct matrix inversion

4.4.5 Boundary conditions

The boundary conditions are discretised for the leftmost nodes only These equations are easily adjusted to give the desired equations for the rightmost nodes

Along line r=0

$$\frac{\partial T}{\partial r} = 0 \qquad \text{Equation 4 32}$$

At node 29

$$0 = \frac{\partial T}{\partial r} \approx \frac{T_{27} - T_{31}}{2H} \Rightarrow T_{31} = T_{27} \qquad \text{Equation 4 33}$$

At node 30

$$0 = \frac{\partial T}{\partial r} \approx \frac{T_{28} - T_{32}}{2H} \Rightarrow T_{32} = T_{28} \qquad \text{Equation 4 34}$$

Boundary between subsystems 1 and 2

$$-k_P \left.\frac{\partial T_{II}}{\partial r}\right|_{r=r_i} = h_1 \left(T_{II}\big|_{r=r_i} - T_B\right)_{average} \qquad \text{Equation 4 35}$$

$$-k_P \left(\frac{T_{21} - T_{23}}{K_{II}}\right) = h_1 (T_{23} - T_B) \qquad \text{Equation 4 36}$$

T_B is found by numerical integration of all the gas nodes in the radial direction at each axial location

Boundary between subsystems 2 and 3

On this boundary, two equations are relevant Condition 1 states in mathematical terms that the heat leaving region 3 at $r=r_a$ is equal to the heat entering region 2 at $r=r_a$ The last term in Condition 2 specifies the heat drop due to imperfect thermal contact between the two regions

$$k_P \left.\frac{\partial T_{II}}{\partial r}\right|_{r=r_o} = k_C \left.\frac{\partial T_{III}}{\partial r}\right|_{r=r_o}$$ Condition 1 (Fourier's Law) Equation 4 37

$$T_{III}\big|_{r=r_o} = T_{II}\big|_{r=r_o} + \frac{k_P}{h_{c1}} \left.\frac{\partial T_{II}}{\partial r}\right|_{r=r_o}$$ Equation 4 38

Condition 2 (Fourier's Law combined with Newton's Law of cooling)

From conditions 1 and 2 above, one arrives at the following for T_{15} and T_{17},

$$T_{17}\left(1+\frac{k_P}{h_{c1}K_{II}}+\frac{K_{III}k_P}{K_{II}k_C}\right)+T_{19}\left(\frac{-k_P}{h_{c1}K_{II}}-\frac{K_{III}k_P}{K_{II}k_C}\right)+T_{13}(-1)=0$$ Equation 4 39

$$T_{15}+T_{13}\left(-\frac{1+\frac{k_P}{h_{c1}K_{II}}}{1+\frac{k_P}{h_{c1}K_{II}}+\frac{K_{III}k_P}{K_{II}k_C}}\right)+T_{19}\left(\frac{\left(1+\frac{k_P}{h_{c1}K_{II}}\right)\left(\frac{k_P}{h_{c1}K_{II}}+\frac{K_{III}k_P}{K_{II}k_C}\right)}{1+\frac{k_P}{h_{c1}K_{II}}+\frac{K_{III}k_P}{K_{II}k_C}}-\frac{-k_P}{h_{c1}K_{II}}\right)=0$$ Equation 4 40

Boundary between subsystems 3 and 4

The following equations are similarly derived for T_7 and T_9

$$T_7\left(1+\frac{k_I}{h_{c2}K_{IV}}+\frac{K_{III}k_I}{K_{IV}k_C}\right)+T_5\left(\frac{-k_I}{h_{c2}K_{IV}}-\frac{K_{III}k_I}{K_{IV}k_C}\right)+T_{11}(-1)=0$$ Equation 4 41

$$T_9 + T_{11}\left(-\frac{1+\frac{k_I}{h_{c2}K_{IV}}}{1+\frac{k_I}{h_{c2}K_{IV}}+\frac{K_{III}k_I}{K_{IV}k_C}}\right)+T_5\left(\frac{\left(1+\frac{k_I}{h_{c2}K_{IV}}\right)\left(\frac{k_I}{h_{c2}K_{IV}}+\frac{K_{III}k_I}{K_{IV}k_C}\right)}{1+\frac{k_I}{h_{c2}K_{IV}}+\frac{K_{III}k_I}{K_{IV}k_C}}-\frac{-k_I}{h_{c2}K_{IV}}\right)=0$$

Equation 4 42

Boundary between subsystem 4 and surrounding air

$$-k_I\left.\frac{\partial T_{IV}}{\partial r}\right|_{r=r_b}=h_2\left(T_{IV}|_{r=r_b}-T_\infty\right)$$

Equation 4 43

$$-k_I\frac{T_1-T_3}{K_{IV}}=h_2\left(T_1-T_\infty\right)$$

Equation 4 44

4.5 MATLAB coding:

"MATLAB is a technical computing environment for high-performance numeric computation and visualisation" [42] Its beauty lies in its ease of programming where the basic data element is a matrix that does not require dimensioning Readily available toolboxes and functions allow a problem to be expressed as they would be mathematically

Row degeneracies occur when one or more of the equations in a linear system is a linear combination of the others There will always be a unique solution as long as there is no row degeneracies A set of equations that are degenerate is called singular [43] While not exact linear combinations of each other, some of the equations may be so close to being linearly dependent that roundoff errors in the machine render them linearly dependent at some stage of the solution process In this case the numerical procedure has failed Accumulated roundoff errors in the solution can swamp the true solution The numerical procedure has not however failed algorithmically The error can be seen by direct substitution back into the original equations

The equations in sections 4 4 1 to 4 4 5 were programmed in the MATLAB environment They are coded in such a way as to allow a variable number of nodes in

the axial and radial directions It was found when coding this particular problem that the A matrix (see equation 4 45) is very close to being singular

$$AT = B \quad \equiv \quad \begin{aligned} a_{11}T_1 + a_{12}T_2 + \quad & + a_{1n}T_n = B_1 \\ a_{21}T_1 + a_{22}T_2 + \quad & + a_{2n}T_n = B_2 \\ & \\ a_{n1}T_1 + a_{n2}T_2 + \quad & + a_{nn}T_n = B_n \end{aligned}$$

Equation 4 45

MATLAB provides an appropriate warning of the condition number of the matrix being extremely large, and the fact that the computed results may be inaccurate In the event that the calculated matrix T is suspected as being wrong, this can be easily verified by direct substitution back into the original equations The closer the equations are to being singular the more likely that T will be inaccurate The use of the MATLAB command $T=A\backslash B$ to solve for T compounds the problem as Gaussian elimination is implemented

In practice the size of the matrix system to be solved is very large as many mesh points are needed for higher degrees of accuracy This stems from the fact that the sensor elliptic boundary value problem produces a large number of conditions that must be satisfied It is wasteful to use general methods of linear algebra on such problems, because most of the arithmetic operations are devoted to solving the set of equations or inverting the matrix involve zero operands It is pointless therefore to reserve memory for unfruitful zero elements Efficiency of algorithms, both in computational load and storage requirements, becomes a principal concern

The sparseness[1] of the system must therefore be utilised, and taken advantage of, as otherwise the problem will become prohibitively large [39] Using sparse matrix techniques, the increasing number of nodes does not present a problem, and different sparse matrix techniques are used to solve for the node temperatures Time and memory space can be saved depending on the type of sparse form Methods for solving sparse systems rely specifically on the form of matrix sparsity present A

[1]A system of linear equations is called *sparse* if a relatively small number of its matrix elements are nonzero See Figure 4 6 Non-zero elements along the main diagonal can be clearly seen

diagonal matrix with fringes is produced as a result of the discretisation. Fringes are nonzero diagonal lines parallel to the main diagonal as can be seen in Figure 4.6.

Speed and efficiency are fundamental issues with regard to all software design. One should endeavour to avoid 'bottleneck' computations that stifle fast program execution. A number of methods are recommended within MATLAB to facilitate a speed increase:

1) Avoid the use of *for* loops. This can be done with the aid of vectorisation techniques. Vector operators are used so that all operations may be performed on each element simultaneously instead of cyclically [44].
2) In the event that a 2D array needs to be initialised, use the *zeros* command *(Method A)* to preallocate and initialise rather than a nested loop structure *(Method B)*. This becomes apparent for very large matrices.

Method A

```
A=zeros(M,N);
```

Method B

```
for i = 1:m,
  for j = 1:n,
    A(i,j) = 0;
end; end;
```

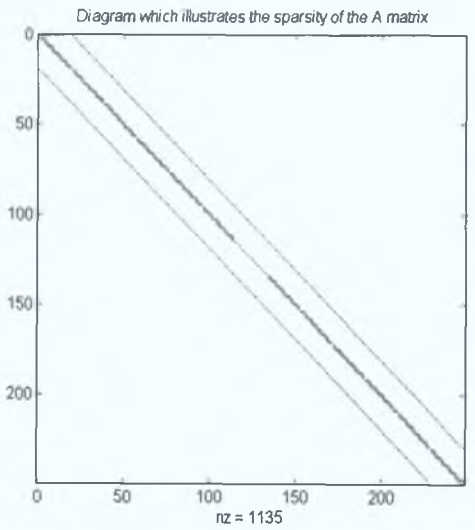

Figure 4.6 Illustration of sparsity of matrix A

3) MATLAB has a built in sparse matrix data type along with many associated algorithms that may be transparent to the users. This serves to greatly reduce computation time for simulation. If a sparse matrix is to be preallocated, using the

spalloc command reduces the time taken of the *zeros* command as memory space is necessary only for nonzero matrix elements. A knock on effect can now be observed in MATLAB. When the systems sparseness is detected, a different algorithm, other than Gaussian elimination, is automatically used to find a system solution using the *A/B* command. The former algorithm proved to be much faster than the standard iterative method known as Gauss-Siedel. (Iterative methods have quick solution convergence). The built in nature of the algorithm into the MATLAB package would also have a bearing on this point. Functions from the Numerical Algorithms Group (NAG) toolbox failed to give any increase in computation speed [45]. Figures 4.7 and 4.8 show the reduction of floating point operations (flops), and the factor of speed increase utilising sparsity.

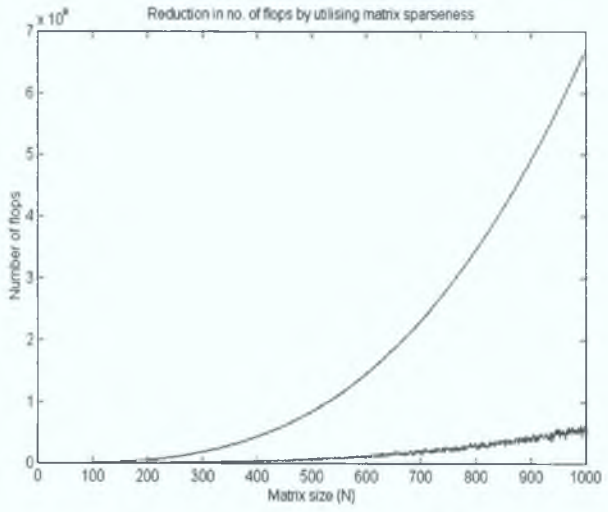

Figure 4.7 Flops reduction in using sparse method

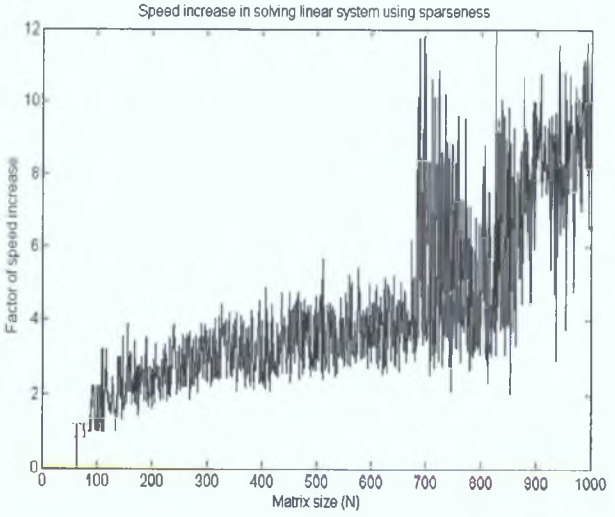

Figure 4.8 Speed increase in using sparse methods

It is very easy to construct a graphical user interface (GUI) for the models using MATLAB One is shown in Figure 4 9 which allows the user to change model type and parameter values without the need for editing and rerunning programs

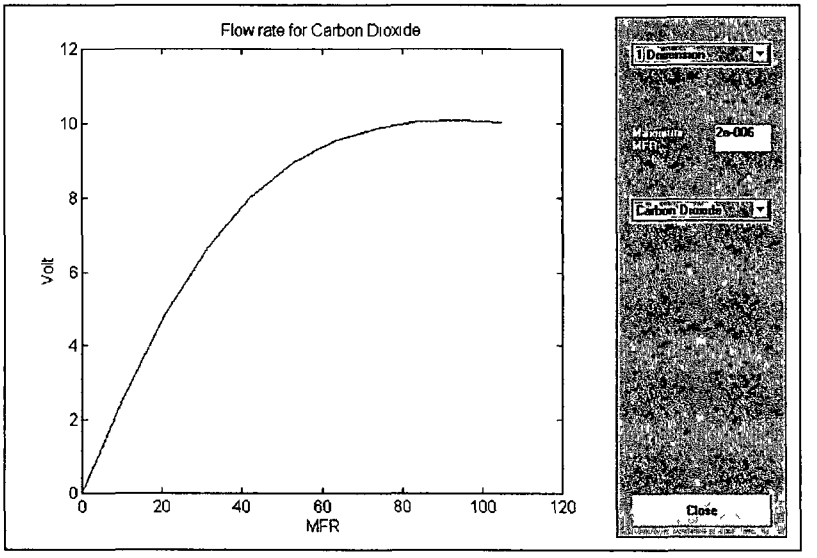

Figure 4.9 GUI for model

4.6 Summary:

This chapter illustrated reasons why a two dimensional model may be more applicable In the derivation of the 2D equations, it can be seen that new parameters such as all of the thermal conductivities and contact coefficients are introduced to the model The effect of these introductions will be shown in the following chapter

It was decided from among the options available to solve the model equations that the cheapest was to write MATLAB programs for a finite difference scheme Some of the most useful commercially available PDE software was discussed A description of how the equations were discretised and coded was included along with some advice and limitations of this method Also briefly mentioned was the fact that MATLAB has to capability to easily develop GUIs for the models

CHAPTER 5

ACQUISITION OF SENSOR DATA

5.1 Introduction

This chapter outlines the characterisation of the MFR versus bridge voltage of the sensor which is needed to validate the previously described models An explanation of the test rig used for this purpose is given along with the associated code for the digital signal processing (DSP) card

5.2 Test rig setup

The test rig was set up as shown in Figure 5 1 below

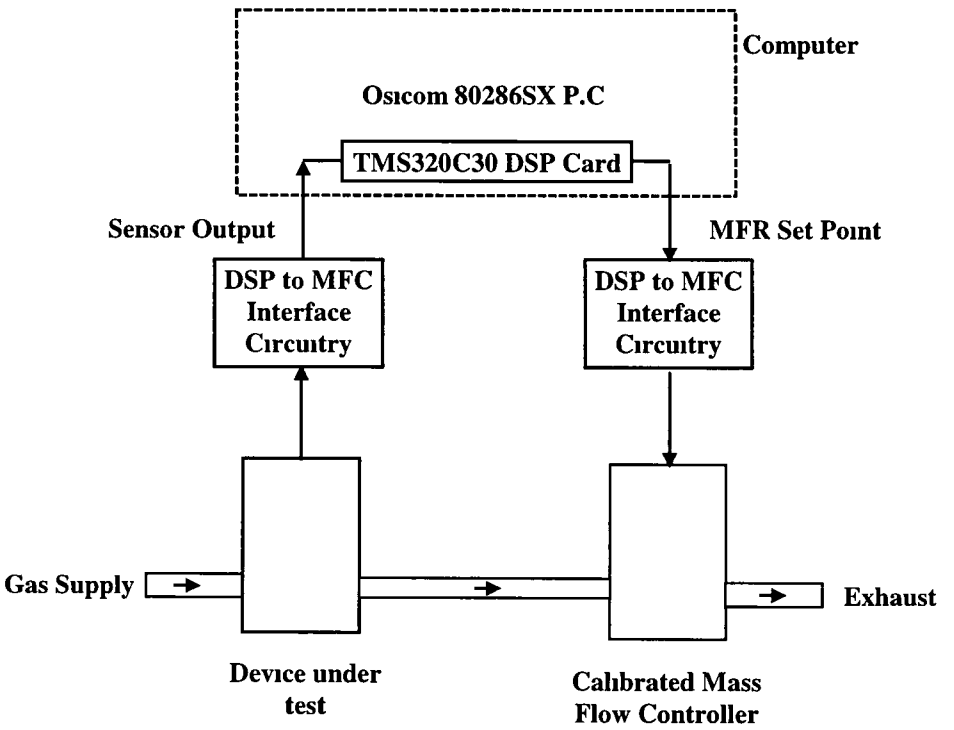

Figure 5.1 Sensor test rig setup

The device under test (DUT) and a MFC are placed in series with the gas supply input. It is important to place the two devices in the above order shown in Figure 5.1, especially when measuring extremely low MFRs as even local air currents may influence readings. See Figure 5.2. The dashed line represents the case where the DUT is downstream of the MFC. This is assumed to be the result of a pressure effect since this is the only change that could occur due to a change in the relative positions of the DUT and the MFC.

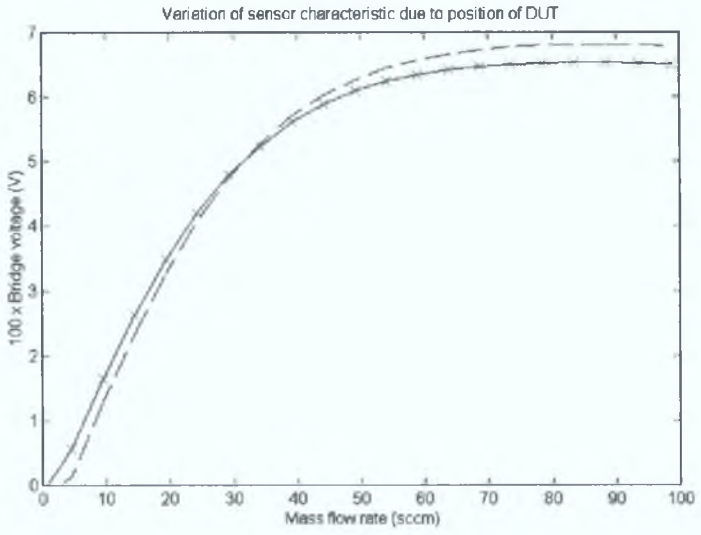

Figure 5.2 Pressure effect on the sensor

The first task involved selecting an existing sensor to be thoroughly tested for static characteristics. An E-Type Unit Instruments sensor was used for this purpose purely for availability reasons. The sensor was incorporated into a Unit Instruments mass flow controller which has its bypass blocked so as to allow only sensor flow. To ensure no control action over mass flow rate by the valve, which is normally closed, 15V was applied to it to keep the valve fully open at all times. This has the effect of breaking the Proportional-Integral-Derivative (PID) feedback control loop in the circuit. The output of the sensor is measured at test point 5 on the printed circuit board, which corresponds to the Wheatstone bridge output voltage amplified by a known factor.

To control the flow through the sensor of each of the test gases used, a mass flow controller (MFC) is used. Ideally the MFC should have the range 0-100sccm, the sensor test range, for maximum accuracy in setpoint readings for each of the different

test gases Since there was access only to an MFC calibrated for Nitrogen alone, tables were used which correlated the MFCs set point to its MFR for various gases Interpolation, by a curve fitting method, was then used to establish intermediate points Test gases used included

Argon, Carbon Dioxide, Carbon Tetrafluoride (CF_4), Helium, Hydrogen, Nitrogen, and Sulphur Hexafluoride (SF_6)

A portable computer incorporating a Loughborough system interface board with the TMS320C30 digital signal processor (DSP) is used to set the flow rate through the sensor, and also to record the output voltage The LSI card is only capable of handling voltages in the range ±3V, so additional scaling was required to convert the above to the range of the MFCs setpoint, 0-5V See Appendix B

5.3 Description of code

5 3 1 Outline

The code used for the TMS320C30 is listed in Appendix C A flow chart representation of the program, and its interrupt subroutine is shown in Figure 5 3 The salient aspects of the code are explained below

5 3 2 Disabling the TMS320C30 card

The CPU/DMA interrupt enable register (IE) is a 32-bit register located in the CPU register file [1] To reset/disable the IE register, all the bits are set to 0 This can be done by logically ANDing 0FFFD with the contents of IE, and placing the result in IE The command *asm* indicates that the assembly language code for the DSP card is to be used Therefore *asm("and 0FFFDh,IE"),* has the effect of disabling the 'C30 card

5 3 3 Enabling the TMS320C30 card

Enabling the card entails using the following assembly language commands

asm("or 2h,IE"),

asm("or 2000h,ST"),

The first command logically ORs a value of 10 (binary) into IE. Bit one is set high to enable external interrupt 1. The second command enables bit 13 of the status register (ST), which represents the Global Interrupt Enable (GIE).

5.3.4 Interrupt subroutine (ISR)

Setting up the ISR involves setting the timer (sampling) period and the routines name:

1. The contents of the Timer Global Control are set to 0x601=11000000001 (binary). Bit 0 configures TCLK as a timer pin. Bit 9 sets up the internal clock which increments the timer to have a period of 120ns. The contents of the Timer Period Register are then set to the desired sampling period divided by the period of the internal clock (120ns). The maximum period allowed is 0xFFFFFFFF*120ns ≈ 515s.
2. Interrupts are handled directly by C functions by using a special naming convention. Interrupt subroutines must have the following name format: **c_int***NN*, where NN is a two-digit interrupt number between 00 and 99. **c_int00** is reserved as the C entry point.

Data may be sent or read from either of two input/output (IO) addresses in the card which are named *A_CHANNEL* and *B_CHANNEL* in the code. When sending data to the digital to analog converters (DACs) an integer value must be used. The floating point value therefore is first converted to an integer, and shifted left 16 bits, as only the top 16 bits are used: **B_CHANNEL=desired_value << 16*

Reading from the analog to digital converters (ADCs) is similar to the DAC "write" process, except that the data is shifted from the top to the bottom 16 bits:
*inA=(*A_CHANNEL) >> 16;*

5.3.5 Writing the output data to file

It is important to remember that there is a time delay of one sample period for both the ADCs and the DACs. This is significant especially in control applications. Since a ramp function is "written" to channel B, there will be a two sample delay between our setpoint and the value read in from channel A.

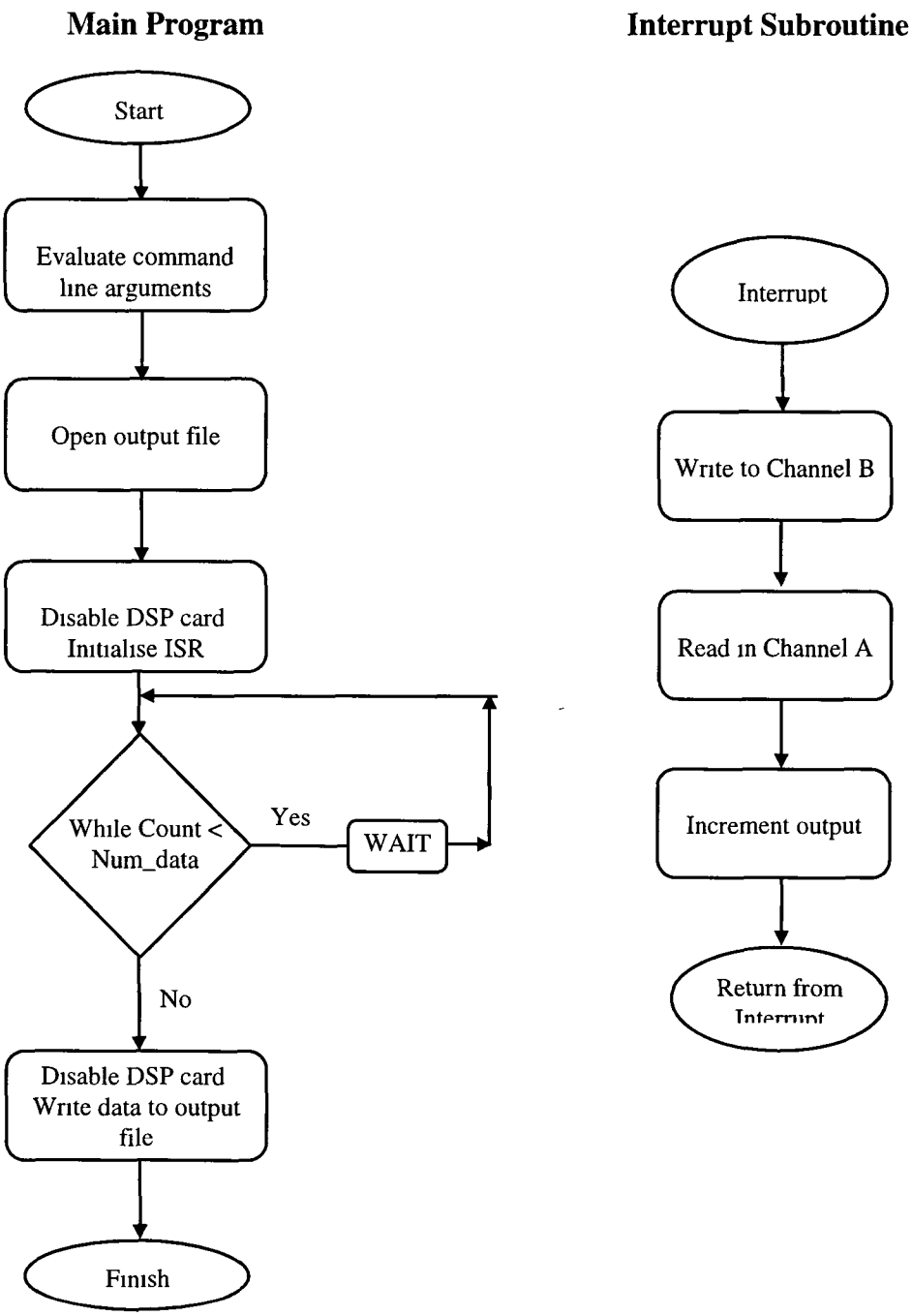

Figure 5.3 Program Flow chart

5.4 Summary

This chapter described the implementation of the sensor test rig The related software has been designed to allow ease of use by specifying command line arguments, which negate the need for time consuming recompilations

CHAPTER 6

VALIDATION

6.1 Introduction

This chapter validates the models developed within chapters 3 & 4 with the data garnered from the test rig explained in chapter 5. Graphs of the experimental data are superimposed on predicted model outputs for comparison purposes. The variation of the prediction between 1D and the 2D models is also compared. To facilitate use of a meter with other gases, flow ratios, also known as 'conversion factors', are normally computed. These factors are computed from the model and compared to published values [20].

Where the meter is used as an integral part of a control loop, there is great need to eliminate its non-linearity (due for the most part to the sensor). To this end, two methods of counteracting it are presented. The first described is the piecewise linear scheme, chosen by Unit Instruments for its commercially available models and the second presents the benefits of developing an inverse function of the output which when multiplied with the output gives a linear system.

6.2 Data obtained for all the gases

A graph of the experimental data is shown in Figure 6.1 for the following gases:

Argon (Ar)
Nitrogen (N_2)
Carbon Dioxide (CO_2)
Sulphur Hexafluoride (SF_6)
Helium (He), Hydrogen (H_2)
Carbon Tetraflouride (CF_4)

This graph highlights the vast difference in the output curves for each of the gases. This is the data which will be used to validate results.

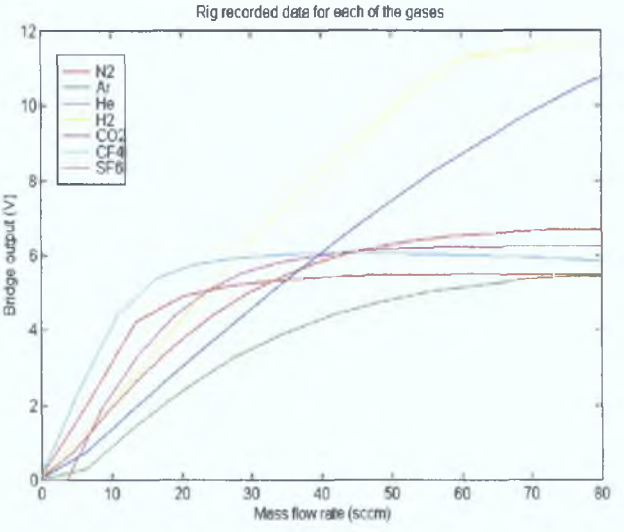

Figure 6.1 Rig data for all gases

6.3 One dimensional results

The following section shows graphs of the recorded data for the gases with the predicted curves from the model. The recorded data is shown in red for all the graphs while the one dimensional model prediction is illustrated in green.

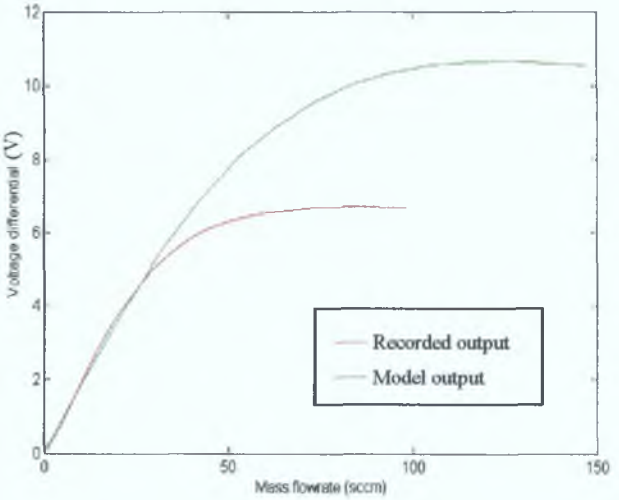

Figure 6.2 Recorded vs Model outputs for Nitrogen

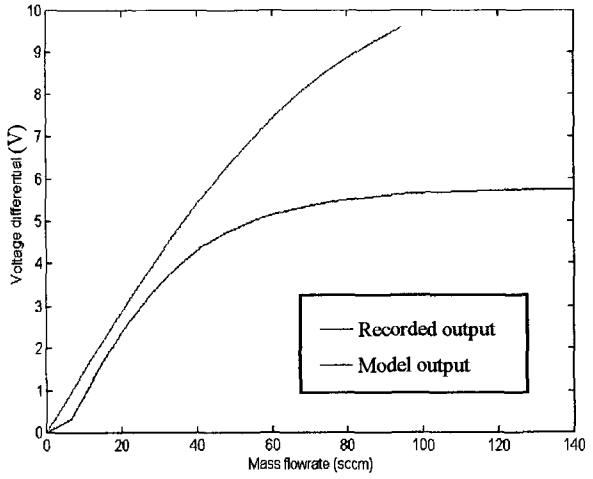

Figure 6.3 Recorded vs Model outputs for Argon

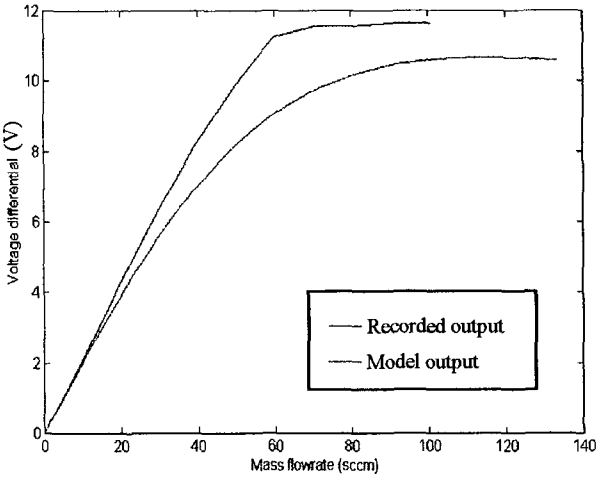

Figure 6.4 Recorded vs Model outputs for Hydrogen

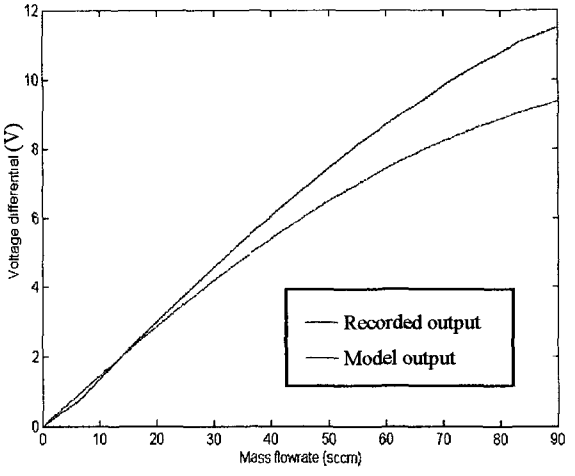

Figure 6.5 Recorded vs Model outputs for Helium

By considering the results obtained from the model, it can be seen that the output curve approaches the output taken from the test rig One can also see that the model output is greater than the rig output for some gases and conversely for others In addition the maximum point of the two curves do not match which would suggest that there is an element of the model, a new term, which may be missing This can not simply be modelled as a 'fudge or correction factor', a constant term times the output, as it is not only a scaling problem Therefore to improve the model, it was expanded to two dimensions in the hope that the new model terms would result in a closer approximation to the measured values

6.4 Two dimensional results

Modelling the system in the radial as well as the axial dimension provided the opportunity to visualise the temperature profile in this dimension and to get an idea of the amount of heat lost from the system Unfortunately the system equations provided by the finite difference method proved to be to unsolvable for the four regions described in Chapter 4 Hence the model was reduced to three regions in assuming that no heat passed from the coils to the insulation Figure 6 6 shows the radial temperature profile of the sensor when an MFR of 100 sccm of nitrogen is passing through it

The model was limited to three regions due to the mathematical capabilities of the chosen solution method, which is not particularly adaptable to problems of high aspect ratios with very distinct and abrupt boundary conditions A first attempt at correcting such problems would involve increasing the number of grid points However, given these particular problems, an increase in the number of grid points is not a feasible option as there were already memory issues associated with getting a solution Using three regions only, and therefore assuming that all the heat from the coils passes inwards through the sensor towards the gas, one can see that there is a virtually no difference between this and the 1D model

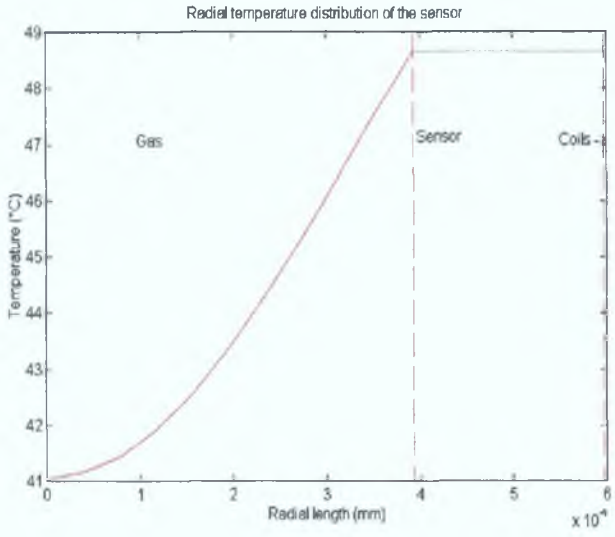

Figure 6.6 Radial temperature distribution

The boundary between the gas and the interior wall of the sensor is easily distinguishable at 3.94mm and shows the abrupt change of the thermal conductivity. By contrast, there is no apparent difference at this resolution at the sensor-coil interface 5.97mm as both the coils and sensor are at the same temperature given the much higher thermal conductivity of both compared to the gas. Indeed, given the fact that the radial temperature profile along the sensor is 'flat', it can be deducted that all the heat is conducted to the gas and that virtually no heat is lost by the sensor itself. This was verified by calculating the amount of the heat supplied along the axial direction which passes from the sensor through to the gas for all mass flow rates and has been found to be almost 100%.

The one-dimensional and two-dimensional models results were then compared to see if any significant change or improvement in the latter over the former. The 2D model results was found to be only very slightly different and represent no significant improvement on the 1D model as the change is practically negligible.

There are a number of reasons for this, most notably the fact that the model is limited to three regions. It would seem that it is necessary to include the insulation layer in the model at least for low flows as the conductivity of the insulation is of the same order as that of the gas at this stage.

An explanation can be given on consideration of the sensor as analogous to an electrical circuit as in Figure 6 7 Each thermal resistance is inversely proportional to the thermal conductivity of the region involved and one can see that the thermal resistance of the gas region is a variable dependant on the mass flow rate Note also that the flow of current in the circuit is analagous to the flow of heat From the diagram, one can see that the thermal resistance of the gas region is low for high mass flow rates and vice versa Therefore, for high flow rates the combined thermal resistance of the gas and sensor regions is of a much lower order of magnitude than that of the insulation region and, as such, the vast majority of the heat ("current") will flow through branch A For the other extreme, allowing for extremely low mass flow rates, the thermal resistances of branches A and B have the same order of magnitude, and so the flow of heat through both is approximately equal

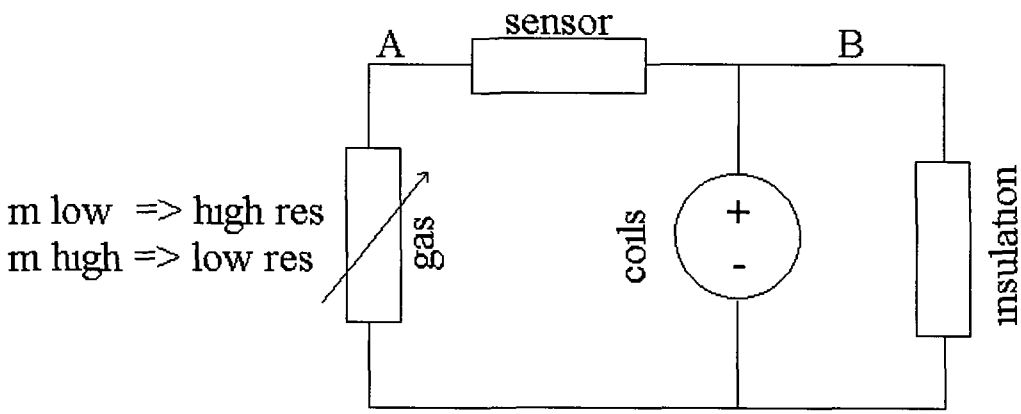

Figure 6.7 Analogous circuit to sensor

If one considers the extreme case where 50% of the heat is lost to the exterior, then as already previously shown, the magnitude of the output will decrease proportionally Given the above fact, one would expect to see a change between the 1D and the 2D models as shown in Figure 6 8 It is difficult to predetermine the mass flow rate at which the effect becomes negligible (100 sccm in the diagram) and also the magnitude of the effect This is the principal failure of the 2D model as it stands and highlights the need to further investigate the effect with regard to loss mass flow rates

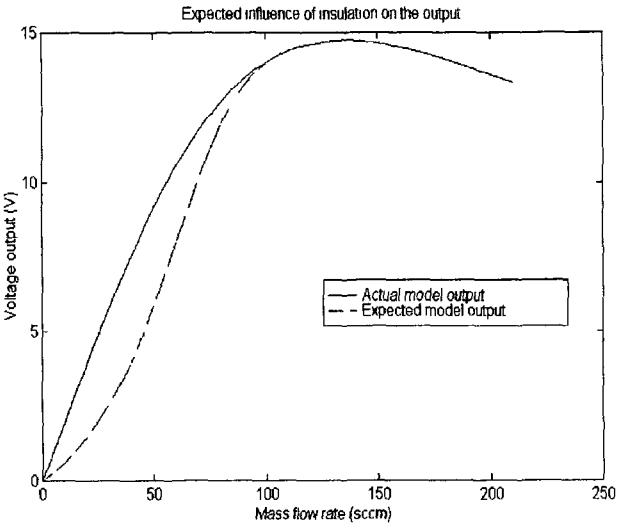

Figure 6.8 Expected influence of insulation

6.5 Flow ratio between gases

Figure 6 9 shows the bridge voltage output of the sensor for both nitrogen and argon gas Any horizontal line drawn across to intersect both curves gives the mass flow rates through the sensor for each of the two gases for this particular output voltage Note that this is only possible up to the maximum output value for argon Dividing m_2 by m_1 for all output values gives what is known as a 'conversion factor' curve

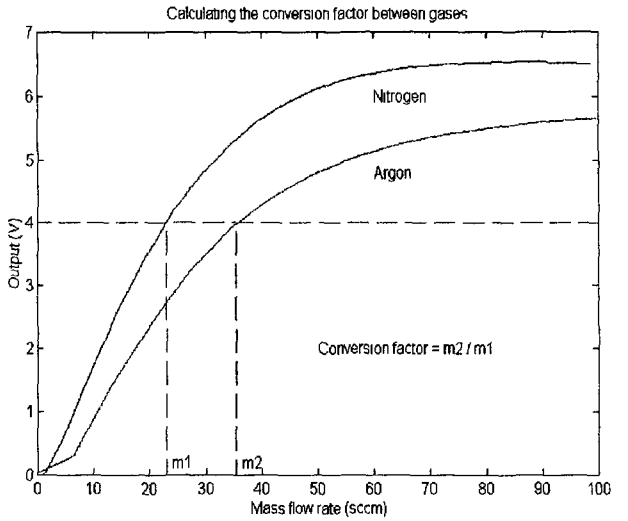

Figure 6.9 Conversion factors' calculation

It can be seen from Figure 6.10 that the conversion factor is a function of the mass flow rate of the two gases. The initial peak seems is a valve effect which may be attributable to stiction at the lower end of valve travel.

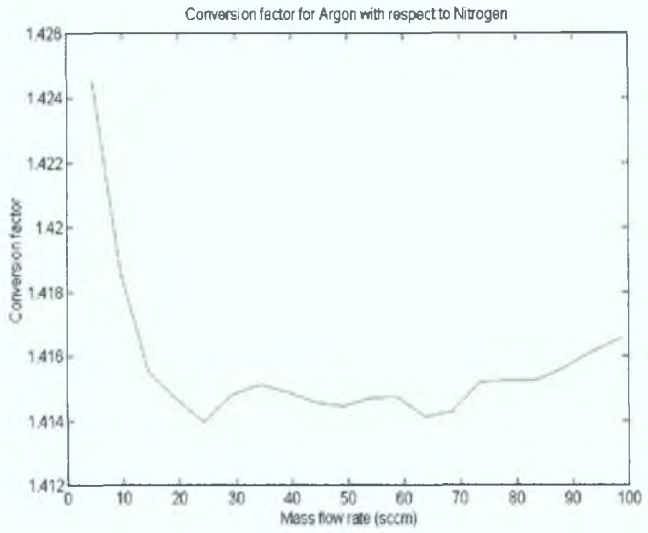

Figure 6.10 Conversion factor for Argon with respect to Nitrogen

It is important to note that this figure is normally only calculated when the units of flow rate are sccm, a figure which is dependent on the mass flow rate and the gas density. A conversion factor based on mass flow rates (kg/s) can be converted to its sccm equivalent by multiplying it by a constant equal to ρ_{Ar}/ρ_{N_2}. The conversion factor (CF) is particularly useful when a sensor has been calibrated for one gas (known as a surrogate) only. In such cases one need only multiply the calibrated output by the CF to find the mass flow rate of the secondary gas. In effect therefore, the sensor is calibrated for all gases for which the CF is known. CFs for all of the test gases are shown below in Figure 6.11. It can be seen that these figures are relatively stable for the range 0-100 sccm.

Conversion values were then computed using the model only and these values proved to be highly inaccurate by at least an order of magnitude given the cumulative effect of the model error for each of the gases. The model values were also found not to be constant over the 100 sccm range used for the experimental data. A much improved model would have to be developed if the predicted conversion factors are to be used in

place of experimentally obtained results However, it is worth noting that CFs are only ever published by Unit Instruments for small degrees of accuracy In the event that higher accuracy is required, meter recalibration is necessary

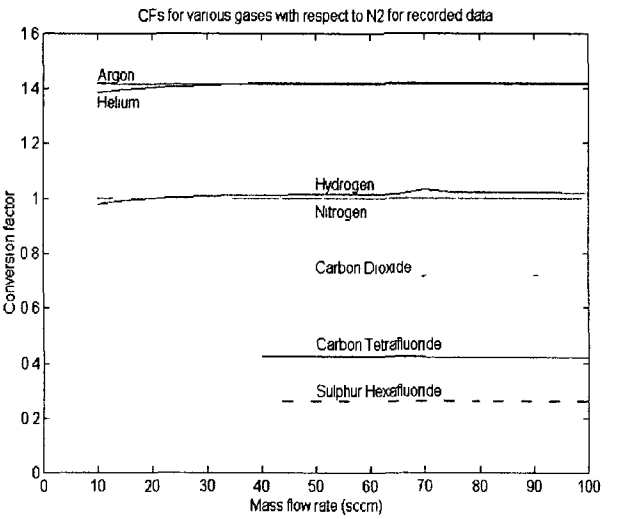

Figure 6.11 CFs for all test gases

6.6 Inverse output function

It has been previously mentioned that the sensor in general practice is only used for measuring limited MFRs (~10 sccm) due to its incorporation in a bypass arrangement This ensures that the linearity of the sensor output voltage is at a maximum prior to further conditioning

Figure 6 12 shows an example of the piecewise linear scheme used by Unit Instruments that can easily be changed to include an increased number of approximating output lines Note that the diagram shows a linearisation over 150 sccm using three lines for clarity as in reality, Unit Instruments use a five line scheme on the first 10 sccm only for increased accuracy

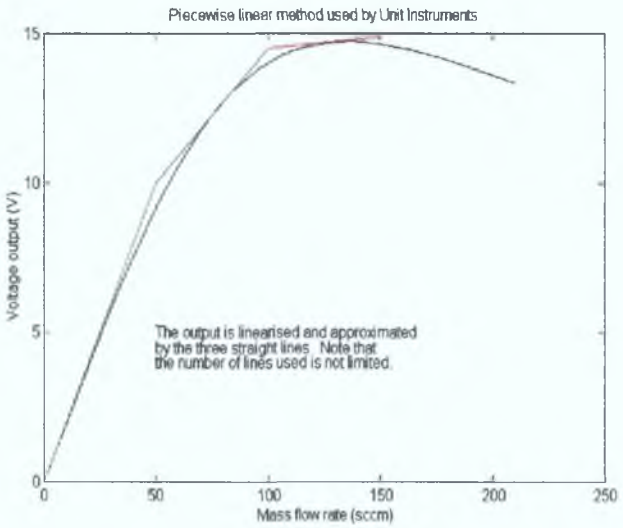

Figure 6.12 Piecewise linearisation

To increase the useful range of the sensor one may utilise an inverse function of the output. A mathematical definition an inverse function can be given by [46]:

> Two functions f:A□B and g:D□E are said to be inverse functions or inverses of each other, provided that,
>
> (i) The domain of each is in the range of the other. A=E and D=B; and
>
> (ii) f(g(x))=x for all x In D and g(f(x))=x for all x in A

If the output is multiplied by its inverse function, one obtains a one to one relationship between the input and output. This is a more useful output form with regard to any control methodology as the system non-linearities are effectively removed. In this case the MFM and its inverse function would be treated as a single linear system as in Figure 6.13. The added benefit in using an inverse function is that the sensor may now be used to measure MFRs greater than that at which the maximum output voltage occurs. The simplest method of finding the function is in finding the reflection of the output in the line $y = x$. This is done by merely interchanging the x and y coordinates on the output curve. A polynomial of any degree can then be fitted to the new coordinates using MATLAB.

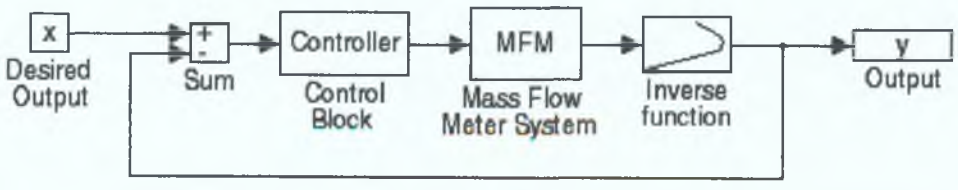

Figure 6.13 Block diagram of a mass flow controller

6.7 Model accuracy

Given the considerable weakness of the model to parameter tolerance, it was decided to show in a visual fashion as in Figure 6 14, for greater effect, the error bounds of the model and thereby present the limitations of the model to date This diagram also includes a trace of the experimental data in between these two limits and the two limits take into account the model's unknown parameters

However, the results do show that the experimental data always lies within the error range of the model and that to this extent, the accuracy of the model is always assured The fact that the maximum value of the experimental data occurs at a lower flowrate than was expected can be explained due to the unknown value of the thermal conductivity of the sensor Conductivities for stainless steels vary considerably and a value was taken based on the stainless steel type which is 316L

As was found earlier when computing conversion factors, the model is not accurate when combining model results of other gases as a multiplication of the error occurs

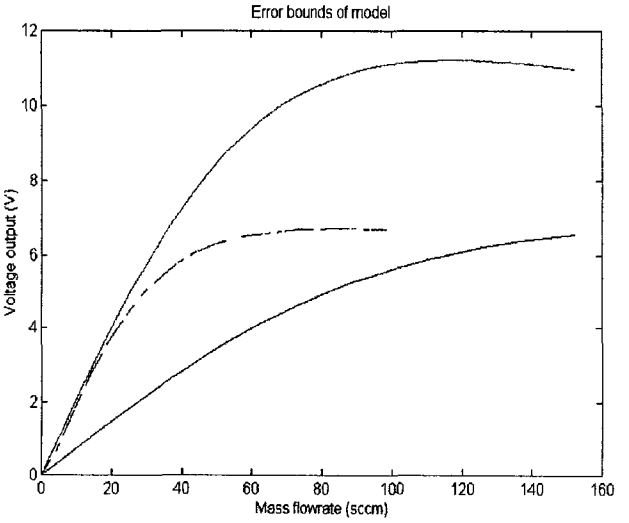

Figure 6.14 Error bounds of model based on parameter tolerence

6.8 Summary :

The results of the 1D model were seen to reproduce the experimental data in shape and form, yet it remained clear that given the difference between both for all of the chosen gases, there were elements which needed to be further analysed and modelled to bring closer together the two sets of results However, from a more optimistic point of view, it is obvious that the modelling was proceeding in the right direction In light of the above need, the model was extended to 2D to take into account the effect of all the previously unmodelled terms

The effect of the gas conductivity on the accuracy of the model was shown to be minimal Reasons for extending the model to include the insulation layer were presented given its effect at low mass flow rates An image of its projected effect is also included and explained

If the sensor is to be used as part of a mass flow control system, the output must be linearised to make use of the simplest control methodologies Unit Instruments given method of piecewise linearising the output curve was presented along with its limitations and an alternative method shown is to compute an inverse function for the output of the sensor for all the gases with the aid of which one can have a perfectly linear system MFMs incorporating the thermal mass flow measurement typically utilise PID controller designs To enable their use in this manner, it is vital that the MFMs output is linear

The model's accuracy may also be complemented by obtaining more precise parameter values, as well as extending the model to include the insulation region The sensitivity of the model to each of its parameters was already presented, and the effect of all these were combined to give worst case error bounds for the model These are very significant and emphasise the limits within which the model can be judged in terms of its precision since the experimental data is clearly to be found between these two limits

CHAPTER 7

CONCLUSIONS AND RECOMMENDATIONS

7.1 Conclusions

This thesis presented in its opening chapters the raison d'être of thermal mass-flow meters for gases and identified the market niche in particular of the most recent addition to this group, the capillary type thermal meter. It was recognised why this type of meter is particularly suited to measuring low quantities of gases for industrial processes. Volumetric type meters were determined to be inherently inaccurate due to their sensitivity to changing ambient pressure and temperature.

Building on the above needs, it was decided to model the thermal meter, as no models for such meters were readily available in any science and engineering journals. At present, all design of these sensors is based on qualitative and accumulated knowledge from experimentation. The sensor is somewhat taken as a 'magical device' with little effort at understanding its dynamics taking place. A model on the other hand helps optimise a meter's design, allows system expertise to be quickly gained and helps reduce design cycle time by predicting the effect of parameter changes. The goal always remains the same: to understand which of the system's characteristics and interactions are essential in order to quantify and represent its behaviour.

The physical construction of the device was outlined in chapter 3 and all aspects of the meter were modelled given that the meter functions as a bypass arrangement. It was initially assumed that the ratio of flow of gas through the capillary to the flow through the bypass is always constant. This assumption was validated for one particular bypass arrangement and it was shown that there are only slight constant deviations which could easily be taken into account by any simple sensor control scheme. A model of the sensor's electronic bridge arrangement was also developed.

At this point the system's 'heart', its sensor, was modelled using the standard heat laws to allow a complete simulation of the mass flow meter. It was decided to begin by modelling in one dimension only. This initiative proved productive in that it provided an output which reproduced published results (without model) and inferred that the approach taken was correct. Using the model as an aid to provide the average coil temperatures for changing flow rate, the output curve was also comprehensively explained. The ability to view temperature distribution of the coils for different flow rates helps improve one's understanding of the sensor's characteristics.

One of the most useful properties of the model is that it allows us to examine the sensor's sensitivity to parameter changes. It was found on a whole that the capillary tube is the single most sensitive element of the sensor and from which it was concluded that any manufacturing process of sensors must concentrate on the radial measurements. The sensor is too sensitive to radial tolerances and using its quoted measurements, the predicted output may increase threefold. This helps explain the need for individual calibration of meters at present. Slight changes in the sensor length (within the tolerances) were shown to have a negligible output effect. Given that a value for the thermal conductivity of the sensor could not be gained from Unit Instruments, this parameter remains unknown and an estimate was used. There is a huge variation in this value for differing stainless steels and on examination of the model equation, one can see that this term is always multiplied by the cross sectional area of the sensor. Hence any variation in this value is of the same order as that for the radial measurement. It was found that changes to the other model parameters, the specific heat capacity and the thermal coefficient of the coils are of lesser sensitivity. Also of use was the fact that accurate values of these quantities were available. The quantity of heat added to the system was concluded to be, to a first approximation, directly proportional to the output.

In general however, the model's output voltage was much higher than expected so different heat distributions were tried to see their effects. Distributing the heat uniformly over the whole of the sensor was seen to be a poor approximation. After discarding the idea of a parabolic distribution for similar reasons, the model was

adjusted to conform closer to reality by heating only a central part of the sensor. This part is 11% of the sensor length for the Unit Instruments sensor. It was found that heating only this fraction lowers the voltage output. However it was found by varying this length within the model that the output has maximum sensitivity when 50% is heated. Having a small gap between the coils was shown to have no output effect as was changing the length of the sensor. Surprisingly, it was shown that the meter is extremely susceptible to changes in ambient temperatures as this was supposedly one of the strengths of the device. Hence this parameter must be taken into account in any future developments. Temperature changes are generally accounted for in the control electronics by means of temperature compensation circuitry. (for e.g. as in Unit Instrument devices.)

To take into account the effect of heat losses and the thermal conductivity of the gases, it was necessary to develop a two dimensional model in the cylindrical coordinate system. Given that the solution of the system of equations was to be obtained by finite difference methods, it was decided to reduce the model to ease its solution. Though the model was fully formed, and since there were no values available for thermal boundary resistances or for the sensor insulation, these parameters were neglected. This was justified in that the sensitivity due to these parameters was negligible with regard to those used in the 1D model and that there was no need for added complexity. Heat loss by radiation was ignored as all system equations resulting from such would have be solved by iteration. The effect of thermal conductivity of the gas was noted as bringing about very little change.

To solve the system of equations involved, it was concluded that the cheapest and fastest method was to write finite difference code to be run in MATLAB, as this package has the added benefits of being widely available and ideally suited for matrix operations. In addition, it contains many useful sparse matrix features which drastically reduce the memory necessary and also the speed of solution. A function based on the Gauss-Siedel algorithm proved to be much slower than what is contained within MATLAB. MATLAB's equation solver was found to be approximately twice as fast as those within the NAG toolbox such as F04ARF and F04ATF.

Beyond a certain point, there was little need in adding extra terms to the 2D model as given their unknown values and their effect There was no benefit in adding extra terms that complicate the model with practically negligible terms Unfortunately it was concluded that the solution of the system for four regions was beyond the scope of the finite difference method and that to advance further a system based on finite element methods needs to be considered

7.2 Recommendations

Any recommendations for future work will obviously entail an increase in model variables and complexity that must have justified reasons for inclusion

1) The first recommendation is as to be expected It is essential to increase the accuracy of the model and to do this one must know the sensor's parameter values as accurately as possible since the model is most sensitive to these values As was demonstrated in the previous chapter, the measured output curve of the meter falls within the considerable error band of the model's associated values Given that the error margin is so high, further development is being impeded and the addition of new parameters is rendered senseless

2) A pressure term could be added into the model given the effects that were seen at low flows in chapter 5 It is obviously not negligible at these levels and it is not known if will have as much of a bearing at higher flow rates

3) Throughout the course of the work described here, the large effect of ambient temperature on the sensor output was shown and merely noted for later investigation To counteract its effect, a 2D lookup table could easily be constructed for the voltage output and the MFR for different temperatures within the MATLAB environment or alternatively one could temperature compensate the associated controllers at a later stage on a printed circuit board

4) The sensor's dynamic characteristics may be modelled by adding a time element to the equations, this would be easily incorporated The greatest difficulty associated with such a task would be gaining the solution to the system For this purpose, the finite difference scheme would not suffice as its limits are already being approached This is evident from the near singularity of the system matrix for four regions

5) The use of Finite Element Methods (FEM) could be considered for this purpose as they are more conducive for more difficult problems To write such code is an immense task and unfortunately such packages to solve generic problems are extremely expensive However the use of FEMs would alleviate the difficulties associated with boundaries In addition, one could practically abandon coding and concentrate on the modelling as opposed to the mathematics involved which is too much of a task in itself Some FEM code is distributed as freeware on the world wide web, so any code resembling the sensor's mathematics could be taken and modified if package funding is available Nevertheless, no known package or code at present allows for changing mass flow rates

6) The next logical step after meter design is to devise a controller Given that the dynamic characteristics would be known, one could readily design the control circuitry for the system It would appear from observation that the sensor behaves as a simple first order system, a fact which could be easily validated The use of a controller with a response time of a higher order of magnitude than that of the sensor would be needed to record the step response For such controllers, the inverse functions mentioned previously are very much applicable

To summarise, it would be worthwhile continuing the development of a 2D model only if the addition of extra model terms need to be investigated Otherwise, the continued use of a 1D model may be considered if improvements are made to both the approximation of the heat input and the heat loss

BIBLIOGRAPHY

[1] *Principles of measurement systems*, Bentley.

[2] *A survey of mass flowmeters*, MP Wilson, Jr., University of Rhode Island, Kingston, Rhode Island, pp 865-870.

[3] *Contemporary college physics*, Jones and Childers

[4] *Fundamentals of flow measurement,* JP DeCarlo, Instrument Society of America 1984.

[5] *Fundamentals of pipe flow,* Benedict.

[6] *Gas flow measurement,* Tony Donnelly & Chris Gimson, Readout Dec94/Jan 95

[7] *Mass Flow Measurement - a state of the art review*, RS Medlock, RA Furness, Measurement and control, Volume 23, May 1990.

[8] Outline - *Sensing and Control*, Honeywell volume 10 - issue 1.

[9] Nov 1992, Chem. Eng., Mass flow meters

[10] 1993 Survey directory, Chem Eng.

[11] *Mass flowmeters* Control & Instrumentation Iss: Survey Directory p. 33, 35
Date: Dec. 1993

[12] *A survey of mass flowmeters* M.P. Wilson, University of Rhode Island.

[13] *Measurement Systems, Application and Design*, Doebelin, E.O., McGraw-Hill 1983.

[14] *Linear momentum mass flowmeter design and performance* Rusnak, J.J., Wuori, E.R., Minell, M.R. Pg 871

[15] *Flowmeters*, Hayward, A., Macmillan Publishers Ltd., 1979.

[16] *Developments in flow measurement,* Scott, R.W.W., Applied Science Publishers Ltd., 1982.

[17] *Process instruments and controls handbook*, Considine.

[18] *Trends in low gas flow metering*, Welch, J.V., Intech, February 1991.

[19] *Handbook of measurement science*, Syndenham, Vol. 2, Pg 1093

[20] Assortment of Unit Instruments brochures http://www.unit.com

[21] Sierra Instruments. http://www.sierrainstruments.com/product.htm

[22] Heated sensors for flow measurement, Wasserman, R., Grant, H, Instruments and control systems, May 1973.

[23] *Survey of thermal devices for measuring flow*, Benson, J H

[24] Process gas mass flow controllers an overview, Olin, J G , Solid State Technology, April 1988

[25] *Instrument Technology*, Jones

[26] Beckwith, T G , Marangoni, R D , Lienhard, J H , Mechanical Measurements Addisson-Wesley Publishing company 1993

[27] *Thermal methods of flow measurement*, J of Physics E 1968

[28] Identification of linear systems

[29]Unit instruments schematics Company confidential

[30] Internal technical report PEI-UL 1995, Jeff Punch

[31] Mechanics of fluids, Massey

[32] *Fundamentals of heat transfer*, Thomas, L C , Prentice-Hall 1980

[33] *An Engineering tutorial Thermal Mass Flowmeters*, Olin, J G , INTECH Engineer's Notebook, PP37-41, volume 40(8), 1993

[34] Kreith, F, Black, W Z , *Basic heat transfer*, Harper, 1980

[35] Kays, W M , Crawford, M E , *Convective heat and mass transfer*, McGraw-Hill, 1980

[36] Heating http //www cad ornl gov/cad_ce/text/htff_overview html

[37] Sinda, http //www sinda com

[38] PDE toolbox http //www mathworks com

[39] Press, W H et al, *Numerical Recipes in C*, Cambridge University Press, 1990

[40] Smith, GH, *Numerical solution of partial differential equations*, Clarendon Press, 1978

[41] Holman, JP, Heat transfer, McGraw-Hill, 1981

[42] MATLAB User Guide Version 4 2 http //www mathworks com

[43] Advanced engineering mathematics, Kreyszig

[44] MATLAB FAQ No 1109, How do I vectorise my code? http //www mathworks com

[45] NAG toolbox http //www mathworks com

[46] Calculus and analytical geometry, Edwards and Perry

APPENDIX A

Bypass to sensor flow ratio test code (MATLAB)

```
% This program demonstrates the validity, or otherwise, of
% assuming that the fraction of the flow in an MFM through
% the sensor is a constant

clear all,
hold off,
dens=0 936,     % Density of Nitrogen
v=0 2209e-4,    % Kinematic viscosity of Nitrogen
Ls=0 0889,      % Length of sensor (3 5")
Rs=3 937e-4,    % Radius of sensor
Lb=0 0254,      % Length of bypass tubes (1")
rb=input('Dia of bypass? '),          % Units 0 001"
Rb=rb*25 4e-6/2, % Radius of bypass

I=input('Number of bypasses? '),      % Number of bypass tubes
tol=1e-16,      % tolerance in computed value of mass flow rate

C1=16*dens*pi*v*Ls,
C2=16*dens*pi*v*Lb,
As=pi*Rs*Rs,
Ab=pi*Rb*Rb,
A=Ab/As,

Ms=[1e-10 1e-8 2 4e-7],

for i=1 length(Ms),

  Mold=0,
  Mnew=10000,
  while abs(Mnew-Mold)>tol,
    Mold=Mnew,
    C3=sqrt( (2 5+C1/Ms(i)) /(1 5+C2*I/(Mold-Ms(i))) ),
    Mnew=Ms(i)*(1+I*A*C3),
    M(i)=Mnew,
    K(i)=(M(i)-Ms(i))/Ms(i),
  end
end

Msccm=(M*60/1 1421)*1e6,        % Total flow in sccm
Msc=(Ms*60/1 1421)*1e6,         % Flow through sensor in sccm

plot(Msc,K),                    % Sensor flow (sccm) v flow ratio
xlabel('Sensor flow (sccm)'),
ylabel('bypass to sensor flow ratio'),
title(['Variation of ratio constant between bypass (',
num2str(I),'*',num2str(rb),' thou) and sensor']),
figure(gcf),

clear A C1 C2 C3 Mold i Mnew tol rb v Ab As
hold on,
plot([Msc(1) Msc(length(Msc))],[K(1) K(length(K))],'r'),
```

APPENDIX B

Diagram of TMS320C30 DSP card interface circuitry

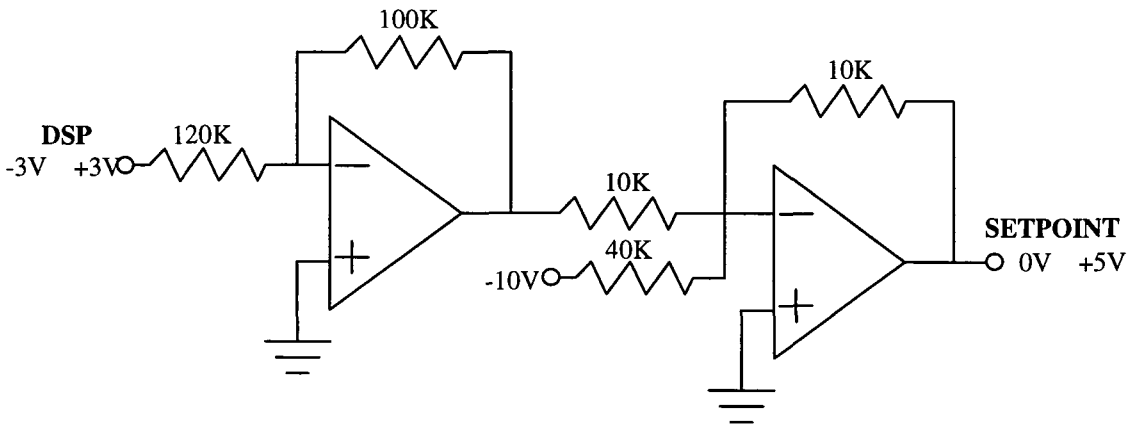

DSP to setpoint on mass flow controller

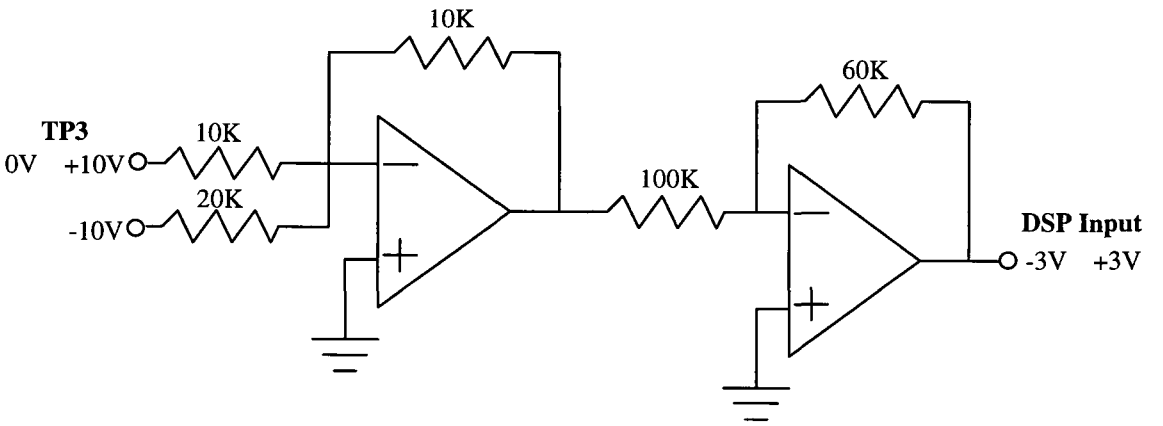

TP3 to DSP card

APPENDIX C

TMS320C30 'C' Code

```
/* ============================================================== */
/*  File:          t.c30

                   Gabriel Duffy

    Description:   This file puts out a ramp signal on channel B
                   and takes back in sensor output on channel A.

                                                                  */
/* ============================================================== */

#include  <math.h>
#include  <stdio.h>
#include  <stdlib.h>

#define   B_CHANNEL     (int*)0x804001    /*Address of Channel B   */
#define   A_CHANNEL     (int*)0x804000    /*Address of Channel A   */
#define   PRIMCTL       (int*)0x808064
#define   EXPCTL        (int*)0x808060
#define   TIME_CTL      (int*)0x808030
#define   TIME_REG      (int*)0x808038

int     num_data=20;       /* Num of data points required. Max=100 */
int     period=300;        /* Sample period (seconds)  Max=515s    */
long int max_value=2*32767; /* Corresponds to 6V span              */

int     des_val[100]={-32767};  /* -3V */
FILE    *fp;
int     inA;
int     outB;
int     in_val[100];
int     max_count;
int     count;
int     increment;
int     i;
float   count_time;
float   volts=5;

void    setup_isr();
void    c_int01();
void    record_data(void);
void    reset(void);
void    disable(void);
void    enable(void);
int     data_count(void);
void    main_body(void);
/*================================================================
                   Interrupt Routine
================================================================*/

void c_int01()
{

 *B_CHANNEL=des_val[count] << 16;  /* Writes to B Channel */
                          /* B must be read first before change */
 inA=(*A_CHANNEL) >> 16;     /* Reads A channel */
```

```
 in_val[count]=inA,
 des_val[count+1]=des_val[count]+increment,
 if (des_val[count+1]>32767)
      des_val[count+1]=32767,
 count++,
}

/*=================================================================
=======
                    Interrupt Handling Functions
=================================================================
=====*/

void disable(void)
{
 asm("  and 0FFFDh,IE   "),
 return,
}

void enable(void)
{
 asm("   or 2h,IE     "),
 asm("   or 2000h,   ST"),
 return,
}

void reset(void)
{
 count=0,
 count_time=0,
 setup_isr(),
 return,
}

void setup_isr()
{
 int *mem,

 disable(),
 *TIME_CTL=0x601,
 *TIME_REG=(1 0*period/120e-9),
 *TIME_CTL=0x6c1,
 asm("    sect  \" int01\""),
 asm("    word _c_int01 "),
 asm("    text   "),
 mem=(int*) 0x2,
 *mem= (int) c_int01,
 enable(),
 }

/*=================================================================
                              Functions
=================================================================*/

void record_data(void)
{
 int i,
 float desired_value,
 float dv,
 float in_value,
 float in_valu,

       printf("\nNow transfering data to file"),
       for (i=0,i<max_count-2,i++)
       {
         desired_value=des_val[i]*3 0/32767,
```

```
         dv=(desired_value+3)*5/6,
         in_value=in_val[i+2]*3 0/32767,
         in_valu=in_value*5/3 + 5 0,
         fprintf(fp,"%4d %8 5f %8 2f %8 5f
%8 5f\n",i,desired_value,dv,in_value,in_valu),
      }
}

void main_body(void)
{
 int temp,

 temp=0,

 printf("\nSample period=%ds",period),
 printf("\nNumber of data points=%d",num_data),
 printf("\nMax value of voltage through D/A and
Ampl's=%7 4fV",volts),

 reset(),
 printf("\nProgram running"),
 while(count<num_data+3)
      {
       /*temp++,*/
      }
 disable(),
 max_count=count,
 record_data(),
 printf("\nData Logged"),
 printf("\nRemember to change name of data file C TXT'"),
 return,
}
/*=====================================================================
                  Main Function
=====================================================================*/

void smain(int argc, char *argv[])
{
 if (argc<3) printf("\nTaking defaults for unspecified values"),
 for(i=1,i<argc,i++){
   if (*(argv[i]++)=='/'){
        switch(*(argv[i]++)){
            case 'p'
            case 'P' period=atoi(argv[i]),
                        break,

            case 'n'
            case 'N' num_data=atoi(argv[i]),
                        break,

            case 'm'
            case 'M' volts=atof(argv[i]),
                        max_value=(long int) abs(volts*2*32767/5),
                        break,

            default  break,}}}

 increment=abs(1 0*max_value/num_data),
 fp = fopen("c txt", "a+"),
 main_body(),
}

 /* End of smain()             */
```

NOMENCLATURE

Symbol	Description	Unit
T	Temperature	°C
T_a	Ambient temperature	°C
L	Length of sensor	m
r	Radius of sensor	m
d	Diameter of sensor	m
x	Fractional length of sensor	-
k	Thermal conductivity	W/m°C
k_g	Thermal conductivity of gas	W/m°C
k_p	Thermal conductivity of pipe	W/m°C
k_c	Thermal conductivity of coils	W/m°C
k_i	Thermal conductivity of insulation	W/m°C
m	mass flow rate	sccm
m_S	mass flow rate through sensor	sccm
m_m	mass flow rate through main meter block	sccm
I	Current	A
V_{OUT}	Bridge output voltage	V
α	Thermal coefficient of resistance	$^{\circ}C^{-1}$
Q	Electrical power input	W
q	Heat input per unit length	W/m
q	Heat input per unit volume	W/m^3
A	Cross-sectional area of a tube or pipe	m^2
C_p	Specific heat capacity	J/(kg °C)
R	Electrical resistance	•
•	Gas density	kg/m^3
C_a	Coriolis acceleration	m/s^2
f	Darcy friction factor	-
g	Acceleration due to gravity	m/s^2
h	Piezometric head loss	m
K	K factor	-
P	Pressure	N/m^2, Pa
Q, q	Volumetric flow rate	m^3/s
H	Grid spacing in axial direction	m
K, K_I, K_{II}, etc	Grid spacing in radial direction	m
	Standard cubic centimetres per second	sccm
	Standard litres per minute	slm